

Published in final edited form as:

*Curr Mol Med.* 2013 December ; 13(10): 1549–1567.

## Quantum Dot-Based Nanoprobes for *In Vivo* Targeted Imaging

Yian Zhu<sup>1</sup>, Hao Hong<sup>2</sup>, Zhi Ping Xu<sup>1</sup>, Zhen Li<sup>3,\*</sup>, and Weibo Cai<sup>2,4,5,\*</sup>

<sup>1</sup> ARC Centre of Excellence for Functional Nanomaterials, Australian Institute for Bioengineering and Nanotechnology, The University of Queensland, Queensland 4072, Australia

<sup>2</sup> Department of Radiology, University of Wisconsin - Madison, Madison, WI, USA

<sup>3</sup> Institute of Superconducting & Electronic Materials, The University of Wollongong, NSW 2500, Australia

<sup>4</sup> Department of Medical Physics, University of Wisconsin - Madison, Madison, WI, USA

<sup>5</sup> University of Wisconsin Carbone Cancer Center, Madison, WI, USA

### Abstract

Fluorescent semiconductor quantum dots (QDs) have attracted tremendous attention over the last decade. The superior optical properties of QDs over conventional organic dyes make them attractive labels for a wide variety of biomedical applications, whereas their potential toxicity and instability in biological environment has puzzled scientific researchers. Much research effort has been devoted to surface modification and functionalization of QDs to make them versatile probes for biomedical applications, and significant progress has been made over the last several years. This review article aims to describe the current state-of-the-art of the synthesis, modification, bioconjugation, and applications of QDs for *in vivo* targeted imaging. In addition, QD-based multifunctional nanoprobes are also summarized.

### Keywords

quantum dots (QDs); nanoparticles (NPs); molecular imaging; cancer nanotechnology; multimodality imaging; near-infrared fluorescence (NIRF)

## 1. INTRODUCTION

Over the last two decades, many imaging tools have been applied in biological and biomedical research, such as magnetic resonance imaging (MRI) [1-3], computed tomography (CT) [4, 5], positron emission tomography (PET) [6-10], single-photon emission computed tomography (SPECT) [11], fluorescence/bioluminescence [12-15], ultrasound (US) [16], as well as multimodality approaches that can combine the benefit of various imaging techniques [17-20]. With the size comparable to biological molecules, but orders of magnitude smaller than human cells, nanoparticles (NPs) can offer unprecedented interactions with biomolecules both on the surface of and inside the cells which may revolutionize disease diagnosis and treatment. Upon incorporation of certain targeting moieties, these NPs can be employed to interrogate specific molecular and cellular events in living systems. For molecular imaging applications, a variety of NPs including magnetic

Weibo Cai, PhD, Departments of Radiology and Medical Physics, University of Wisconsin - Madison, Room 7137, 1111 Highland Avenue, Madison, WI 53705-2275, USA [wcai@uwhealth.org](mailto:wcai@uwhealth.org); Phone: 608-262-1749; Fax: 608-265-0614. Zhen Li, PhD, Institute of Superconducting and Electronic Materials, Australian Institute of Innovative Materials, University of Wollongong, Squires Way, North wollongong, NSW 2500, Australia [zhenl@uow.edu.au](mailto:zhenl@uow.edu.au); Phone: 61-2-4221-5163; Fax: 61-2-4221-5731.

NPs [21-23], semiconductor quantum dots (QDs) [24-28], carbon nanotubes [29-31], gold NPs [32-34], and graphene-based nanomaterials [35-37] have been investigated and are expected to play increasingly more important roles in preclinical/clinical research in the future. Among these NPs, semiconductor QDs have attracted significant attention for optical imaging applications, because of their exceptional properties and many advantages over conventional organic dyes [38].

In general, QDs are semiconductor nanocrystals composed of II-IV (e.g. CdSe and CdTe) or III-V (e.g. InP and InAs) groups of elements. At the nanoscale, the band-gap energy in semiconductors depends not only on the composition of the elements, but also on the particle size [39-42]. Such size dependence, defined as the “quantum confinement effect”, gives rise to unique optical and electronic properties of QDs. Previous reports have demonstrated that by varying the composition and particle size, QDs with a wide range of absorption and emission wavelengths from the visible to the near-infrared (NIR) region can be synthesized [43-45]. A number of features make QDs highly attractive for fluorescence imaging, such as wide absorption range, narrow and symmetric emission spectra, high quantum yields (QY; up to >90%), long fluorescence lifetime (> 10 ns), large effective Stokes shift (> 200 nm), and high resistance to photobleaching and chemical degradation [38]. The small size and high QY endow QDs with high sensitivity, making them suitable for single molecule tracking. The combination of size-tunable fluorescence, large Stokes shifts, and narrow emission spectrum makes it possible to separate the fluorescence signals from different QDs for multiplexed imaging. Because of the high photostability, QDs have also been widely used for long-term imaging studies [46].

Although QDs have many advantages in imaging and spectroscopy, as mentioned above, many barriers exist that can hinder the broad use of QDs for bioimaging applications [47]. For example, the potential toxicity caused by the release of heavy metal ions remains a major concern for QD-based agents [48-50]. In addition, pH-sensitive photoluminescence and prolonged retention in animal studies are also undesirable characteristics that need to be overcome [51-53]. To address these issues, decorating the surface of QDs with biocompatible molecules such as polymers, liposomes, or inorganic silica have been investigated [54-56]. To achieve specific targeting, QDs need to be conjugated to targeting ligands such as peptides, proteins, nucleotides, among others. For *in vivo* imaging applications, the following factors need to be taken into account when designing the probes: potential toxicity at the effective doses for imaging, interference with or from normal biology/physiology, circulation lifetime, optimal excitation/emission wavelength for sufficient tissue penetration of signal, chemistry for ligand-conjugation and avoiding non-specific trapping, cost effectiveness, etc.

In this review article, we will summarize the recent progress in the use of QD-based nanoprobes for imaging applications, in particular molecularly targeted imaging in animal models. First, we will give a brief overview of the synthesis and surface modification strategies which can render QDs suitable for biomedical applications. Next, we will discuss in detail the use of QD-based agents for *in vivo* targeted imaging. Various examples of QD-based multifunctional nanoprobes for *in vivo* dual-modality imaging will also be illustrated. Lastly, we will discuss the challenges and future directions for applications of QDs in the biomedical arena.

## 2. SYNTHESIS AND SURFACE MODIFICATION OF QDS

### 2.1. Synthesis of QDs

Since the first report of QD synthesis about three decades ago [39], a variety of synthetic methods have been developed for the preparation of QDs. Based on the different media

used, these methods can be broadly classified into two types: the organometallic route [57-60] and aqueous synthesis [61-63]. In a typical organometallic synthesis of QDs, a solvent with high boiling point and high coordinating capability to both metal and chalcogen elements is used, such as trioctylphosphine oxide (TOPO). QDs synthesized in these organic solvents possess nearly perfect crystal structures, and thus high fluorescence QY. Narrow size distribution is another advantage for QDs prepared via this route. On the other hand, the hydrophobic surface of QDs synthesized using this method is a major obstacle for biological applications. Many strategies such as ligand-exchange and coating with a water-soluble shell have been adopted to change the surface properties of QDs, however at the cost of significant loss in fluorescence signal. Another disadvantage of the organometallic route is the costly and laborious synthetic process.

In contrast, aqueous synthesis, with the advantages of improved simplicity/reproducibility and less toxicity, has gradually become a preferred option, despite the lower QY and broader size distribution [64, 65]. For example, hydrophilic thiol-capped QDs are more suitable for biomedical applications because of their higher stability and better compatibility in biological environment compared to those prepared in organic solvent. Recently, various methods have been reported for the synthesis of thiol-capped QDs, including hydrothermal synthesis, ultrasonic methods, and those that use illumination or microwave irradiation [66-69].

The composition, size, and shape of QD core are essential to their photoluminescence emission range, which can be tuned from visible to the NIR range. In addition, the cores of QDs are typically coated with another semiconductor shell composed of materials with lower toxicity and wider band-gap (e.g. ZnS) [70, 71]. The presence of such a shell can not only improve the photoluminescence properties and passivate the surface traps, but also prevent the leaching of the highly toxic heavy metal ions from the QDs [72].

To date, CdSe/ZnS [25, 73-80] and CdTe/ZnS [81-83] QDs are among the most widely investigated QDs for *in vivo* imaging, partly due to their commercial availability and mature synthetic procedure. Meanwhile, there are also many studies using CdTe/CdS, CdHgTe, and PbS QDs [84-87], which are attractive for *in vivo* applications because of their NIR emission. To avoid the use of Cd, since it is one of the most toxic elements, many groups have reported the synthesis and evaluation of InAs/InP/ZnSe [26, 88], CuInS<sub>2</sub>/ZnS [89, 90], CuInSe/ZnS [91], and silicon QDs [92], which will be discussed in more detail in the following text. Recently, photoluminescent carbon-based NPs have also attracted significant attention [93]. Prepared by laser ablation or electrochemical oxidation of carbon targets [94, 95], these luminescent carbon NPs are also subjected to the quantum confinement effects hence are called carbon QDs or C-dots. The strong sustained fluorescence of these C-dots in mice, together with their biocompatibility and non-toxic features, make C-dots an exciting new class of probes for optical imaging [96].

## 2.2. Surface Modification of QDs

Surface modification of QDs can improve the aqueous solubility, especially for those synthesized via the organometallic route, as well as protect them from degradation and fluorescence quenching. In addition, certain surface modification (e.g. with polyethylene glycol [PEG]) can also help to reduce non-specific uptake in normal organs and provide functional groups for further bioconjugation.

PEG coating, because of its well-known biocompatibility and mature chemistry, is one of the most commonly used strategies for surface modification of QDs. Many literature reports have shown that PEG coating can change the biodistribution of QDs in animals [97, 98]. For example, All-Jamal et al. reported that PEG-lipid coated QDs exhibited much longer blood

circulation half-life than the unmodified QDs after systemic administration [97]. In another study, it was demonstrated that PEGylation can reduce the uptake of QDs into organs of the reticuloendothelial system (RES), such as the liver and spleen [98].

Surface modification of QDs with a combination of PEG and other polymers has also been investigated. In an early study, Gao et al. reported the use of an ABC triblock copolymer in addition to PEG for QD coating, aiming to minimize the aggregation and fluorescence loss of QDs when they are stored in physiological buffer or injected into live animals [25]. Various experiments in cells and animal models confirmed the good stability and brightness of these QDs. In another report by Zintchenko et al., a new type of quantoplexes incorporating NIR-emitting CdTe QDs, polyethylenimine (PEI), and plasmid DNA (pDNA) were assembled [99]. Upon intravenous injection, the quantoplexes accumulated rapidly in the lung, liver, and spleen, and the fluorescence signal could be detected for at least a week. Tracking of these quantoplexes immediately after intravenous injection revealed a rapid redistribution from the lung to the liver, which was dependent on the PEI topology and the quantoplex formulation. In addition, a similar quantoplex was also assembled where the PEI was replaced by PEG-PEI conjugate, which exhibited passive tumor accumulation in nude mice bearing subcutaneous tumors. Using a solid dispersion technique, hydrophobic PCDA (10,12-pentacosadiynoic acid) was incorporated to assemble QDs-loaded micelles [100]. In this design, both PEG-PCDA and PCDA-Herceptin conjugates participated in the micelle assembly, which was subjected to intra-micellar cross-linking between PCDAs upon UV irradiation. Non-invasive fluorescent imaging showed that with Herceptin as the targeting ligand for human epidermal growth factor receptor 2 (HER2), these QD-loaded micelles exhibited high anti-tumor activity and selective toxicity, which led to a marked reduction in tumor volume.

In addition to PEG, other polymeric coatings such as poly (lactic-co-glycolic acid) (PLGA) and liposomes have also been explored [84, 101, 102]. For example, *in vivo* experiments demonstrated the increased stability of QD-entrapped nanospheres, between 100 and 200 nm in size, against photooxidation and photobleaching [101]. In another report, the QD-drug-liposome hybrid was found to exhibit greater uptake in mouse brains and lower uptake in the heart and liver compared to free QDs [102]. Recently, an amphiphilic polymer with hydrophobic inner core, termed as *N*-succinyl-*N'*-octyl nanomicelles (SOC), was used to incorporate oil-soluble PbS QDs for subsequent long-term tracking *in vivo* [84].

Inorganic silica is a class of highly biocompatible material that is regularly used as a food additive. Encapsulating QDs within silica can provide a hydrophilic surface and facilitate the incorporation of various functional groups such as carboxyl, amine, and thiol groups for further bioconjugation [103, 104]. Furthermore, silica shell can prevent the release of toxic QD components into the biological environment [72, 105]. Although very few silica-coated QDs (QD-SiO<sub>2</sub>) have been reported for *in vivo* targeted imaging to date, there are several studies focusing on the toxicity and biodistribution assessment. In one report, liver and kidneys were found to be the main target organs for QD-SiO<sub>2</sub> [106]. It was suggested that QD-SiO<sub>2</sub> were metabolized via three pathways according to their distinct aggregated states *in vivo*. A fraction of QD-SiO<sub>2</sub> kept their original form and could be filtered by glomerular capillaries and excreted via urine within five days. Most QD-SiO<sub>2</sub>, adsorbed onto proteins and aggregated into larger particles, were metabolized in the liver and excreted via the feces. Part of the aggregates remained in the hepatic tissue for a prolonged time period and could not be readily cleared. When compared with commercially available QDs (Invitrogen, CA) of similar size and emission wavelength, it was found that QD-SiO<sub>2</sub> exhibited a different biodistribution pattern [107]. The commercially available QDs from Invitrogen showed predominant liver and spleen uptake shortly after intravenous injection, whereas QD-SiO<sub>2</sub>

exhibited much lower liver and spleen uptake but higher kidney uptake, blood retention, and partial renal clearance.

### 2.3. Strategies for Conjugation of QDs with Biomolecules

To effectively recognize and enable non-invasive imaging of specific molecular targets in various organisms, QDs need to be conjugated with ligands that can specifically bind to or interact with the target of interest [108, 109]. Taking into account the surface properties of QDs and the functional groups within the selected targeting ligands, a number of different conjugation strategies can be employed.

Two general approaches can be adopted for QDs with hydrophobic surfaces, which are typically prepared via the organometallic route. These QDs need to be first rendered hydrophilic through either surface ligand exchange [90, 110] or interaction with amphiphilic polymers [111]. Subsequent conjugation of biomolecules to the QDs can be achieved during the ligand exchange step by introducing thiolated biomolecules, which is quite straightforward to obtain QD bioconjugates. However, there are many concerns about the stability and luminescent properties of the resulting QD bioconjugates. For those QDs with amphiphilic polymer as the surface cap, a step of coupling the biomolecules to the polymer is needed [112]. With hydrophilic surfaces, these QDs share similar conjugation strategies with the QDs synthesized via the aqueous route. Based on the functional groups on the QD surface, different reactions can be used for surface conjugation of QDs (**Fig. (1)**).

Ethyl(dimethylaminopropyl) carbodiimide (EDC), one of the most widely used coupling reagents for amide bond formation between carboxylic acid and amino groups, has been commonly used for surface modification of QDs (**Fig. (1A)**) [113]. It has also been used to produce QD-streptavidin conjugates for subsequent binding of biotinylated molecules [114]. However, EDC coupling can cause non-specific crosslinking, since there can be multiple carboxylic acid groups and amino groups in a single biomolecule, which may lead to a loss of bioactivity especially when the carboxylic acid and/or amino groups are involved in the biological function. Compared to EDC coupling, the thiol-maleimide reaction is more specific, since typically only the thiol is present on the biomolecule but not the maleimide. For example, amino groups on the QD surface can be converted to maleimide by reaction with a crosslinker, succinimidyl-4-(N-maleimidomethyl) cyclohexane-1-carboxylate (SMCC), which is then conjugated to thiolated peptides, cysteine-tagged proteins, or partially reduced antibodies via the thiol-maleimide reaction (**Fig. (1B)**).

Another commonly used strategy for functionalization of QDs is through the (strept)avidin-biotin interaction, which is attractive because of its high affinity and specificity [115-117]. This method relies on either direct binding between streptavidin-functionalized QDs with biotinylated proteins/peptides (**Fig. (1C)**), or the use of avidin as a bridge between biotinylated QDs and biomolecules. Metal-histidine binding has also been investigated for surface modification of QDs, in which nickel nitrilotriacetic acid (Ni-NTA, a compound widely used for isolation and purification of proteins that contain histidine tags) groups were introduced [118-120]. For example, QDs can be modified with Ni-NTA groups via EDC coupling, and subsequent metal affinity interactions can allow a stoichiometry-controlled binding of this complex to oligohistidine-tagged proteins (**Fig. (1D)**).

Besides the abovementioned strategies, electrostatic interactions have also been used for conjugating amine-containing dihydrolipoic acid (DHLA) derivative-modified QDs with hyaluronic acid [121]. In addition, several protein-mediated strategies have been reported for bioconjugation of QDs, and one of which involves a commercially available engineered haloalkane dehalogenase called the HaloTag protein (HTP) [122, 123]. HTP in its native form can covalently bind to a synthetic HaloTag ligand (HTL) through the formation of an

ester bond between the chloroalkane within the HTL and the Asp<sup>106</sup> residue of the protein, as shown in **Fig. (2A)**. A critical mutation in the catalytic triad (His<sup>272</sup> to Phe) of HTP can cease further hydrolysis of the newly formed ester bond between HTP and HTL, thereby leading to permanent linkage of the HTL to HTP. In a report by Zhang et al. [124], an engineered Renilla luciferase (Luc8) was genetically fused to the N terminus of HTP and expressed to obtain the fusion protein HTP-Luc8. After conjugating QDs with a HTL, irreversible covalent binding between the HTL-conjugated QDs and HTP-Luc8 led to close proximity of Luc8 and QDs and subsequent bioluminescence resonance energy transfer (BRET, **Fig. (2A)**), which can have many potential applications.

In an intriguing report, intein-mediated protein splicing (a process that takes place after mRNA has been translated into a protein) was used for surface modification of QDs for multiparameter imaging of cellular function [125]. Typically composed of three segments: N-extein, intein, and C-extein, intein can also excise itself and rejoin the remaining portions (N-extein and C-extein) with a peptide bond. In this study, various proteins were genetically tagged with the N-terminal half of a split intein (I<sub>N</sub>) or the C-terminal half (I<sub>C</sub>), whereas the complementary half of the intein was biotinylated and conjugated to streptavidin-coated QDs [125]. Intein-mediated splicing led to simultaneous, site-specific conjugation of QDs to multiple protein targets, which opened up new possibilities for bioimaging applications (**Fig. (2B)**).

### 3. IN VIVO TARGETED IMAGING WITH QDS

Different from passive targeting, which typically depends on the enhanced permeability and retention (EPR) effect for accumulation in the tumor [1, 126, 127], active targeting can be achieved by attaching various targeting ligands to QDs for recognition of specific cell surface molecules or proteins. A wide variety of targeting ligands have been investigated for in vivo targeted imaging with QDs, as we discuss in detail below.

#### 3.1. In Vivo Kinetics of QDs

An ideal fluorescence probe for non-invasive *in vivo* targeted imaging should satisfy several requirements, which include sufficiently long circulating lifetime, minimal non-specific uptake in the RES, sustained fluorescence within the period of a given study, high biocompatibility and low toxicity, among others. A large number of literature reports have indicated that particle size and surface coating are both important factors that can affect the *in vivo* behavior of QDs [48, 54, 98, 106, 128-131].

In an early report, QDs with different surface coatings were investigated with fluorescence imaging in living mice [128]. It was found that the circulation lifetime of QDs depends on the chain length of the surface PEG coating. When QDs were coated with 5 kDa methoxyl-PEG, the circulation half-life was more than 1 h, compared to less than 12 min for QDs with shorter PEG coating. In addition, PEG coating also allowed for fluorescence detection of QDs for at least four months *in vivo* after intravenous injection. In a later report, it was found that QDs of different sizes have different clearance pattern in mice [129]. As shown in **Fig. (3)**, fluorescence signal from QDs of 4.36 nm in diameter was mainly found in the bladder at 4 h after intravenous injection. However, at the same time point, QDs of 8.65 nm in diameter accumulated primarily in the lung, spleen, and liver, indicating a different excretion pattern (i.e. hepatobiliary). It was concluded that to achieve efficient urinary excretion and elimination of QDs, the overall size should be strictly controlled under 5.5 nm. Another possibility is to use biodegradable QDs that can be broken down into renal clearable components, which may be developed in the future. In another study, Praetner et al. provided experimental evidence for faster deposition of carboxyl-coated QDs over

amine-coated or PEG-coated QDs in various tissues, which might be attributed to the interactions between carboxyl-coated QDs and capillary endothelium [132].

### 3.2. Peptide-Conjugated QDs

Peptides are desirable targeting ligands for NPs because of their small sizes, hence a large number of peptides can be attached to a single NP such as QD to enhance the avidity and specificity. Other advantages of peptides include ease of synthesis, low immunogenicity, and tolerance to a variety of reaction conditions, among others. The first report on *in vivo* investigation of peptide-conjugated QDs appeared more than a decade ago [73], in which three peptides were evaluated for *in vivo* targeting of CdSe/ZnS QDs. Subsequently, the arginine-glycine-aspartate (RGD) peptide has been widely used in QD-based research because of its high affinity for integrins  $\alpha_3$  and  $\alpha_5$  [79, 81, 88, 133, 134]. Integrin  $\alpha_3$  is overexpressed on the surface of angiogenic endothelial cells and certain tumor cells [135, 136], which makes it an attractive target for QD-based nanoprobes since extravasation is not required to achieve tumor contrast. The first *in vivo* targeted imaging using peptide-conjugated QDs was reported in 2006 [81]. As shown in **Fig. (4)**, fluorescence signal in the integrin  $\alpha_3$ -positive U87MG tumors could be observed shortly after intravenous injection and peaked at a few hours post-injection, indicating effective integrin  $\alpha_3$  targeting of RGD-conjugated QD705 (with peak emission at 705 nm in the NIR range) in living mice. Detailed histological examination of the tumor tissue revealed that targeting was vascular integrin  $\alpha_3$  specific with little extravasation. Over the last several years, many studies from other research groups have also demonstrated that RGD peptide-conjugated QDs could exhibit highly specific tumor targeting and reduced accumulation in the lung, kidney, and heart in mice models [86, 137-140].

RGD peptides have been conjugated to Cd-free QDs [88, 92, 140], which have much lower potential toxicity and may find broader biomedical applications for future clinical translation. For example, PEGylated InAs/InP/ZnSe QDs were conjugated to either RGD or RAD (Arg-Ala-Asp, which does not bind to integrin  $\alpha_3$ ) peptides and compared, which showed much higher tumor uptake for RGD-conjugated QDs than RAD-conjugated QDs [88]. In another study, RGD peptides were conjugated to PEGylated silicon QDs (SiQDs), which were successfully used for *in vivo* tumor targeting, sentinel lymph node mapping, and multiplexed NIR imaging (**Fig. (5)**) [92]. Recently, InP/ZnS QDs were first coated with biocompatible dendron for a pilot toxicity evaluation in mice [140], which had not only low toxicity at the dose tested but also enhanced passive targeting to tumors. After conjugation to RGD peptides, significantly higher tumor uptake and longer retention at the tumor sites was observed compared to non-targeted dendron-coated QDs.

### 3.3. Proteins as Targeting Ligands for QDs

**3.3.1. Antibodies**—Antibodies are a class of diverse and widely used specific ligands for targeted imaging and therapy. In 2004, Gao et al. reported the conjugation of QDs to a monoclonal antibody recognizing the prostate-specific membrane antigen (PSMA) [25], which was investigated for active tumor targeting in xenograft-bearing mice. Subsequently, several other antibodies have also been conjugated to QDs and tested for tumor targeting *in vivo*, such as an anti-AFP (alpha-fetoprotein) antibody and Herceptin (anti-HER2) [74, 100, 141]. In a comparison study, the AVE-1642 antibody that binds to the insulin-like growth factor 1 receptor (IGF1R, an emerging targeting for cancer imaging and therapy [142]) was used as the targeting ligand for both QDs and AlexaFluor 680 [143]. Whole-body imaging of tumor-bearing mice indicated much higher tumor uptake of AVE-1642-AlexaFluor 680 than the AVE-1642-QD conjugate, which is more likely to be engulfed by macrophages in the RES.

Mesothelin, a tumor differentiation antigen, is normally expressed on the mesothelial cells lining the pleura, peritoneum, and pericardium [144]. Although the biological functions of mesothelin remain to be fully elucidated, overexpression of mesothelin has been found in several human cancer types such as malignant mesothelioma, pancreatic, ovarian, and lung adenocarcinoma. In addition, limited expression of mesothelin in normal tissues makes it highly attractive for specific tumor targeting [144]. In one report, CdTe/ZnS QDs were encapsulated into carboxylated amphiphilic triblock polymer F127 (F127COOH) micelles, which were conjugated to an anti-mesothelin antibody (Me) for tumor targeting *in vivo* [82]. Non-invasive imaging of tumor-bearing mice showed that Me-F127COOH-QD micelles accumulated at the pancreatic tumor site soon after intravenous injection (**Fig. (6)**).

The epidermal growth factor receptor (EGFR) is another extensively studied transmembrane protein, which has a high degree of homology with HER2 [145, 146]. Studies have shown that ~90% of oral squamous cell carcinoma (OSCC) and head and neck squamous cell carcinoma (HNSCC) expresses EGFR at a very high level [147, 148]. Therefore, anti-EGFR antibodies have attracted significant interest for imaging and therapy of OSCC and HNSCC. For example, an anti-EGFR monoclonal antibody was conjugated to QD800, which enabled clear in-situ and *in vivo* imaging of HNSCC [149]. An anti-EGFR antibody was conjugated to Au:CdHgTe QD840 in another study [86], where QD800-RGD and QD820-anti-CEACAM1 (carcinoembryonic antigen-related cell adhesion molecule-1) conjugates were also synthesized and used together with QD840-anti-EGFR for *in vivo* tumor targeting in human lung adenocarcinoma xenografts. It was demonstrated that all three tumor markers (EGFR, integrin  $\alpha_3$ , and CEACAM1) could be detected simultaneously, after spectral unmixing of the fluorescence signal from the three different QD conjugates.

**3.3.2. Antibody Fragments**—Although many monoclonal antibodies have been used for QD-based tumor targeting and imaging, the relatively large size of antibodies limits the number of ligands that can be attached to the surface of each QD. In addition, it may also hamper the penetration into solid tumors, which typically have high interstitial pressure. Alternatively, single-chain antibody fragments (ScFv), consisted of antibody heavy- and light-chain variable domains connected by a flexible peptide linker, is a much smaller targeting ligand than intact antibodies (25 kDa vs. 150 kDa) which can maintain high binding affinity and specificity to the antigen [150]. In one report, ScFvEGFR was conjugated to either QDs or magnetic iron oxide (IO) NPs for *in vivo* tumor targeting and imaging in an orthotopic pancreatic cancer model [76]. Cytoplasmic localization of ScFvEGFR-QDs was observed as fluorescent clusters, suggesting that cellular uptake of ScFvEGFR-QDs was likely via receptor-mediated internalization. In addition, markedly reduced uptake of ScFvEGFR-QDs was observed in the liver and spleen when compared to mice injected with non-targeted QDs.

The glucose-regulated protein GRP78, a member of the heat shock protein family that plays critical roles in cancer cell proliferation and oncogenesis/angiogenesis, has been shown to bind  $\text{Ca}^{2+}$  and serve as an endoplasmic reticulum (ER) stress signaling regulator [151]. Recently, ScFvGRP78 was used as targeting ligands for QD conjugation, which exhibited effective inhibition of breast tumor growth in a mouse model [152]. c-Met, a receptor tyrosine kinase that is strongly associated with cancer cell proliferation, migration, invasion, and tumor angiogenesis, has attracted significant attention for targeted cancer therapy [153, 154]. In a recent study, an anti-c-Met ScFv (Ms20) was conjugated to doxorubicin-loaded PEGylated liposomes (LD) as well as QDs [78]. *In vivo* tumor targeted imaging (with Ms20-QDs) and cancer therapy (with Ms20-LD) were both successfully achieved.

**3.3.3. Other Proteins**—Many other proteins besides antibodies can have strong affinity to specific targets/receptors, such as EGF (i.e. epidermal growth factor) which is the naturally



occurring ligand for EGFR [146]. In an interesting study, the distribution of EGF-QDs was compared with unconjugated QDs through three distinct phases: tumor influx (~3 min), clearance (~60 min), and accumulation (1-6 h) [75]. Both QDs and EGF-QDs behaved similarly at ~60 min, with comparable non-specific and rapid tumor influx and clearance, followed by an apparent dynamic equilibrium. However, EGF-QDs progressively accumulated in the tumors between 1 and 6 h, whereas tumoral concentration of non-targeted QDs gradually decreased during this period. At 24 h after injection, tumor fluorescence of either QDs or EGF-QDs was minimal and not readily detectable. In another report, specific EGFR targeting with  $^{99m}\text{Tc}$ -labeled, EGF-conjugated QDs was reported in a breast cancer model, which allowed for monitoring of EGFR downregulation upon therapy [155].

Successful delivery of imaging agents to the brain is highly important for both diagnosis and treatment of central nervous system (CNS) diseases [3, 156]. However, the blood-brain barrier (BBB), formed by tight junctions within the capillary endothelium, is a major obstacle for successful brain imaging. The wheat germ agglutinin (WGA), isolated from *Triticum vulgare*, belongs to the lectin families and can bind specifically to sugar molecules such as N-acetyl-D-glucosamine and sialic acid. By specifically recognizing sugar molecules, WGA-conjugated QDs were shown to be capable of binding to glycosylated components on cell surface [157, 158]. After intranasal administration of WGA-QDs into BALB/c mice, WGA was reported to enhance the binding of WGA-QDs with nasal mucosa and further improve their uptake in the brain, which peaked at a few hours after administration (**Fig. (7)**). Such brain targeting and imaging characteristics of WGA-QDs makes it a promising nanoplatform for future imaging of various CNS diseases.

### 3.4. Other Ligands for *In Vivo* Targeting of QDs

With many advantages including small size, versatile chemistry, ease of synthesis, and lack of immunogenicity, aptamers have recently emerged as a new class of targeting ligands for molecular imaging and therapy [159, 160]. Although aptamers have been conjugated to many types of imaging agents such as organic dyes, magnetic NPs, and gold NPs, investigation of aptamer-conjugated QDs is mainly in the *in vitro* setting [161-163]. To the best of our knowledge, there is only one literature report on *in vivo* imaging and therapy of cancer using QD-aptamer conjugates [164]. To achieve active ovarian cancer targeting, QDs was conjugated with a DNA aptamer specific for MUC1 (mucin 1, a cell surface associated mucin which is overexpressed in many cancer types) via EDC coupling. In addition, doxorubicin (DOX, a commonly used anti-cancer drug) was attached to QDs via a pH-sensitive hydrazine bond, which is stable in the circulation but can be cleaved and release DOX in acidic environment, such as after internalization into cancer cells. *In vivo* imaging experiments revealed significantly higher tumor accumulation of the targeted QD conjugate than the non-targeted QDs [164].

The folate receptor (FR), also called folate-binding protein, is a glycosylphosphatidylinositol-anchored protein that specifically binds folic acid and folate-conjugated molecules. The alpha isoform of FR (FR- $\alpha$ ) is found to be overexpressed in many epithelial cancers but not highly expressed in normal tissues except the kidneys. Since the affinity of FR for folic acid and folate conjugates is relatively high ( $K_d$  of ~100 pM), FR- $\alpha$  has been extensively investigated for tumor targeting [165], including many studies focusing on QDs [80, 83, 85, 89, 166, 167]. For example, folic acid was conjugated to PEG and subsequently deposited onto *N*-acetyl-L-cysteine (NAC)-stabilized CdTeS alloyed QDs, which was demonstrated to be capable of tumor targeting in mouse models [167]. Non-Cd-containing CuInS<sub>2</sub>/ZnS QDs with folate-modified N-succinyl-N'-octyl chitosan (FA-SOC) micelles have also been reported [89]. It was shown that the oil-soluble QDs could be

effectively dispersed in water and served as a platform for tumor targeting and imaging (**Fig. (8)**).

Hyaluronic acid (HA, also known as hyaluronan or hyaluronate), an anionic non-sulfated glycosaminoglycan that is widely distributed throughout connective, epithelial, and neural tissues, has been conjugated to QDs for tumor targeting since HA was shown to be associated with tumor angiogenesis and progression [168]. Since HA can specifically bind CD44, a cell-surface glycoprotein overexpressed in many tumor types, HA-QDs were found to have not only cancer targeting characteristics, but also the capability for imaging lymphatic vessels [121]. In another study, carbohydrate capped QDs were prepared by conjugating PEGylated QDs with D-mannose or D-galactosamine, which was tested for *in vitro* imaging and *in vivo* liver targeting [169]. Captopril is a drug for treating hypertension since it can inhibit the activity of angiotensin-converting enzyme. The *in vivo* behavior of captopril-conjugated QDs has been investigated after intraperitoneal injection [77]. Strikingly, it could be delivered into the brain via systemic circulation, suggesting that it may be a potential platform to break the BBB. Besides the above mentioned ligands for QD conjugation, DOX has also been conjugated to QDs for targeting alveolar macrophages and inflammation [170].

#### 4. DUAL-MODALITY IMAGING WITH QD-BASED NANOPROBES

Tremendous advances have been made in many imaging techniques over the last decade, not only in the clinical arena but also in preclinical imaging systems. However, no single imaging modality is perfect to obtain all the necessary information for a given study. For instance, fluorescence imaging faces the challenge of quantification and deep tissue penetration. MRI has superb soft tissue contrast and good resolution but suffers from poor sensitivity. Although PET is superior in sensitivity, quantitation, and tissue penetration, its resolution is relatively low. Combination of multiple imaging techniques using a single probe can potentially overcome these disadvantages and provide synergistic information. Many QD-based nanoprobcs have been designed and evaluated for these applications.

##### 4.1. Fluorescence/MRI

In an early report, Mulder et al. coated QDs with paramagnetic gadolinium complexes and PEGylated lipids to develop a dual-modality probe for both fluorescence imaging and MRI, using the RGD peptides as ligands for tumor targeting [171]. However, the dual-modality probe was only tested *in vitro*. Cho et al. reported a multifunctional nanocarrier composed of fluorescent QDs, superparamagnetic IO NPs, an anti-PSMA antibody, and chemotherapeutic agent paclitaxel [172]. Although a series of experiments confirmed the safety and tumor-targeting capability of the nanocarrier, more studies need to be carried out in the future to fully realize its potential for dual-modality imaging.

In 2011, Tan et al. assembled a multimodal system by co-encapsulating IO NPs and QDs in NPs composed of poly (lactic acid)-d- $\alpha$ -tocopheryl polyethylene glycol 1000 succinate [173]. Without using any targeting ligands, the passive tumor targeting characteristics of the system was demonstrated by both MRI and fluorescence imaging. Breast cancer associated antigen 1 (BRCA1) is overexpressed in ~65% clinical specimens of gastric cancer tissues as well as several gastric cancer cell lines. Wang et al. reported fluorescence imaging and MRI of gastric cancer using BRCA1 as the target [174]. By conjugating fluorescent magnetic NPs with an antibody that binds to BRCA1, gastric cancer targeted imaging was carried out in tumor-bearing nude mice.

Recently, a core/shell nanoprobe was constructed for dual-modality imaging of breast cancer, which was composed of an IO NP core and two outside layers of silica shell [175].

CdSe/ZnS QDs (with emission peak at 600 nm) and NIR fluorescent CdSeTe/CdS QDs (with emission peak at 780 nm) were embedded inside each silica layer to form the dual-modality agent which was termed as MQQ-probe. After conjugation with an anti-HER2 antibody, the HER2-MQQ-probe was injected into tumor-bearing mice. NIR fluorescence imaging demonstrated enhanced tumor specific accumulation of HER2-MQQ-probe than the non-targeted MQQ-probe. Meanwhile, MRI provided detailed anatomical structure of the tumor.

#### 4.2. Fluorescence/CT

X-ray computed tomography (CT) is one of the most reliable and widely used diagnostic tools in the clinic, which is fast, three-dimensional (3D), and has high spatial resolution [1, 5]. Traditional clinical contrast agents for CT are based on iodinated molecules and compounds with high X-ray absorption coefficient. However, these contrast agents are typically cleared very rapidly from the blood or lymphatic vessels, which is a major disadvantage. Cardiovascular disease is a leading cause of death worldwide, and unstable atherosclerotic plaques represent important diagnostic targets in clinical settings for improving patient management [176, 177]. Recently, fluorescent QDs were combined with iodinated molecules to create a dual-modality contrast agent, which can potentially confer the advantages of both CT and optical imaging [178]. This nanoemulsion platform, composed of a hydrophobic iodinated oil core with QDs embedded inside, was demonstrated to have good fluorescence and X-ray absorption abilities both *in vitro* and *in vivo*, which can be used for targeting macrophages in atherosclerotic plaques.

#### 4.3. Fluorescence/PET

PET is another widely used imaging technique in cancer diagnosis, staging, and evaluation of therapeutic efficacy due to its high sensitivity, good quantitation capability, and superb tissue penetration of signal [7, 179-182]. In 2007, we reported the first targeted dual-modality fluorescence/PET probe based on QDs, where  $^{64}\text{Cu}$  was used to label QDs through the DOTA (1,4,7,10-tetraazacyclododecane- $N,N',N'',N'''$ -tetraacetic acid) chelator and the RGD peptide was employed as the targeting ligand [183]. DOTA-QD-RGD exhibited integrin  $\alpha_v\beta_3$ -specific binding in cell culture and in U87MG tumor-bearing mice, which had significantly higher uptake than the non-targeted QDs. Based on PET imaging, the U87MG tumor-to-muscle ratios for  $^{64}\text{Cu}$ -DOTA-QD-RGD and  $^{64}\text{Cu}$ -DOTA-QD were about 4:1 and 1:1, respectively. Excellent linear correlation was obtained between the results measured by *in vivo* PET imaging and those measured by *ex vivo* NIRF imaging or tissue homogenate fluorescence. Histology examination revealed that DOTA-QD-RGD targets primarily the tumor vasculature with little extravasation, similar as the previous report using RGD-conjugated QDs without  $^{64}\text{Cu}$ -labeling [81]. Subsequently, an analogous dual-modality probe targeting the vascular endothelial growth factor receptor (VEGFR) was also developed in a similar fashion, using VEGF as the targeting ligand (**Fig. (9)**) [184]. Again, vascular specific targeting of QDs was observed with little to no extravasation.

### 5. CONCLUSION AND FUTURE PERSPECTIVES

For imaging purposes, nanotechnology has touched upon every single modality of the molecular imaging arena. Among the various types of NPs, QDs are one of the most intensively studied which possess many inherent advantages over traditional fluorescent dyes such as significantly higher brightness, tunable and narrow emission spectra, and increased photostability. Robust chemistry for surface modification and targeting ligand conjugation is of critical importance to the potential applications of QDs. Over the last decade, versatile chemistry has been developed for synthesis and functionalization of QDs for *in vitro* and *in vivo* imaging.

Despite the remarkable progress over the last 2 decades, many obstacles exist for wide spread use of QD-based imaging agents and potential clinical translation. For example, the potential toxicity of QDs is still a major concern, due to the chemical composition of toxic elements such as Cd, Se, Hg, Pb, As, etc. Although many studies have demonstrated the safety of QDs in animal models, their long-term effect needs to be fully elucidated. To avoid these issues, researchers have developed and investigated Cd-free QDs such as CuInS<sub>2</sub> QDs, SiQDs, C-dots etc., which showed promising results as described above. Another way to improve the stability of QDs and thereby reducing the potential toxicity is through the use of optimized surface coating. It has been demonstrated that various biocompatible polymers can effectively protect QDs from degradation in biological environment. However, these coatings can result in significantly increased overall size of QDs and can markedly affect the *in vivo* distribution, excretion, and metabolism. Therefore, there is still a need for new surface coating strategies, with which the overall size of QD-based nanoprobe can be strictly controlled in addition to effective protection of QDs from biological environment. In addition, the current methods used for conjugation of targeting ligands to QDs are suboptimal in several aspects such as low efficiency, cross-reactivity, and strong dependence on the conditions and materials used. Development of more efficient, specific, versatile, and straightforward conjugation strategies is needed in future research.

One of the key challenges for QD-based imaging agents is (tumor) targeting efficacy. We believe that tumor vasculature (instead of tumor cell) targeting should be the best bet for QDs since many of the QD-based probes reported in the literature suffered from poor extravasation when compared with small molecules or proteins [185, 186]. Aside from oncology, QD-based agents may also find broad applications in imaging of cardiovascular diseases since the targets are immediately accessible upon intravenous injection. The use of molecularly targeted QDs can provide multiple advantages over small molecule-based agents, which include stronger signal (due to the superb brightness of QDs over fluorescent dyes), enhanced binding affinity and specificity to the target (attributed to multivalency with the presence of a large number of targeting ligands), etc.

When using QDs for *in vivo* targeted imaging, the choice of targeting ligand is very important. Among the different classes of specific ligands, peptides/small molecules are more desirable when compared with antibodies/proteins since they can keep the overall size small, are easier to synthesize, are more stable and resistant to harsh reaction conditions, and can fully take advantage of the multivalency effect since more peptides/small molecules can be attached to each QD than antibodies/proteins. Furthermore, antibodies, proteins, and antibody fragments typically require the use of complicated biological expression systems for their production, and the separation of conjugated QDs from antibodies/proteins can be challenging due to their similar size. Although DNA/RNA aptamers are also easy to produce/synthesize and can have less interactions with proteins *in vivo* than antibodies/proteins (i.e. lower background signal), the affinity for individual target is usually quite low. In theory, QDs are large enough to enable multiple targeting ligands on the surface of a single QD to simultaneously bind to multiple targets. However, this aspect has been virtually unexplored to date. Targeting multiple different but closely-related receptors (e.g. VEGFR and integrin  $\alpha_3$ ) by incorporating different targeting ligands on the same QD, with spacers of suitable length, require robust chemistry to minimize batch-to-batch difference and improve reproducibility.

The emerging field of multimodality imaging with QD-based nanoprobe can allow researchers to detect the same NP with multiple imaging techniques. Cross-modality validation is critical for providing more accurate and reliable data than with fluorescence imaging alone. Although optical imaging can offer high sensitivity (nM level) to complement MRI (mM level) and MRI can bypass the signal penetration limitation of

optical imaging, the combination of optical and MRI is not optimal since neither modality is quantitative. Dual-modality QD-based agents that combine PET (which is very sensitive and highly quantitative) and optical imaging (which can significantly facilitate *ex vivo* validation of the *in vivo* data) should be of particular interest for future biomedical applications. For multimodal imaging employing more than two techniques, a PET/MRI/optical agent is perhaps the most useful since such a combination provides superb sensitivity (PET), quantitation capability (PET), excellent anatomical information and soft tissue contrast (MRI), as well as a means for *ex vivo* validation (optical) which itself can also be useful for highly sensitive imaging in certain clinically relevant scenarios (e.g. superficial tissue, endoscopy, and intra-operative guidance).

The bright future of nanomedicine lies partly in multifunctional nanoplatfoms which combine both therapeutic components and multimodality imaging, often called “theranostics” [187-189]. The ultimate goal of theranostic nanomedicine is that NP-based agents can allow for efficient, specific *in vivo* delivery of therapeutic agents (drugs, genes, etc.) without systemic toxicity, and the dose delivered as well as the therapeutic efficacy can be accurately measured non-invasively over time. Much future research effort will be needed before this can be a clinical reality. Continuous multidisciplinary efforts on the development and optimization of such nanoplatfoms will shed new light on molecular diagnostics and molecular therapy, and newer generation of QD-based nanoplatfoms may have the potential to profoundly impact disease diagnosis and patient management in the near future.

## Acknowledgments

This work is supported, in part, by the University of Wisconsin - Madison, the National Institutes of Health (NIBIB/NCI 1R01CA169365), the Department of Defense (W81XWH-11-1-0644), and the American Cancer Society (RSG-13-099-01-CCE).

## References

1. James ML, Gambhir SS. A molecular imaging primer: modalities, imaging agents, and applications. *Physiol Rev.* 2012; 92:897–965. [PubMed: 22535898]
2. Sosnovik DE, Weissleder R. Emerging concepts in molecular MRI. *Curr Opin Biotechnol.* 2007; 18:4–10. [PubMed: 17126545]
3. Balyasnikova S, Lofgren J, de Nijs R, et al. PET/MR in oncology: an introduction with focus on MR and future perspectives for hybrid imaging. *Am J Nucl Med Mol Imaging.* 2012; 2:458–74. [PubMed: 23145362]
4. Bhargava P, He G, Samarghandi A, Delpassand ES. Pictorial review of SPECT/CT imaging applications in clinical nuclear medicine. *Am J Nucl Med Mol Imaging.* 2012; 2:221–31. [PubMed: 23133813]
5. Tejwani A, Lavaf A, Parikh K, et al. The role of PET/CT in decreasing inter-observer variability in treatment planning and evaluation of response for cervical cancer. *Am J Nucl Med Mol Imaging.* 2012; 2:307–13. [PubMed: 23133818]
6. Gambhir SS, Czernin J, Schwimmer J, et al. A tabulated summary of the FDG PET literature. *J Nucl Med.* 2001; 42:1S–93S. [PubMed: 11483694]
7. Gambhir SS. Molecular imaging of cancer with positron emission tomography. *Nat Rev Cancer.* 2002; 2:683–93. [PubMed: 12209157]
8. Iagaru A. <sup>18</sup>F-FDG PET/CT: timing for evaluation of response to therapy remains a clinical challenge. *Am J Nucl Med Mol Imaging.* 2011; 1:63–4. [PubMed: 23133796]
9. Cai W, Hong H. Peptoid and Positron Emission Tomography: an Appealing Combination. *Am J Nucl Med Mol Imaging.* 2011; 1:76–9. [PubMed: 22022661]
10. Li D, Shan H, Conti P, Li Z. PET imaging of metabotropic glutamate receptor subtype 5 (mGluR5). *Am J Nucl Med Mol Imaging.* 2012; 2:29–32. [PubMed: 23133800]

11. Fakhri GE. Ready for prime time? Dual tracer PET and SPECT imaging. *Am J Nucl Med Mol Imaging*. 2012; 2:415–7. [PubMed: 23145358]
12. Huang X, Lee S, Chen X. Design of “smart” probes for optical imaging of apoptosis. *Am J Nucl Med Mol Imaging*. 2011; 1:3–17. [PubMed: 22514789]
13. Gaikwad SM, Ray P. Non-invasive imaging of PI3K/Akt/mTOR signalling in cancer. *Am J Nucl Med Mol Imaging*. 2012; 2:418–31. [PubMed: 23145359]
14. Cai W, Zhang Y, Kamp TJ. Imaging of Induced Pluripotent Stem Cells: From Cellular Reprogramming to Transplantation. *Am J Nucl Med Mol Imaging*. 2011; 1:18–28. [PubMed: 21841970]
15. Chin PT, Beekman CA, Buckle T, Josephson L, van Leeuwen FW. Multispectral visualization of surgical safety-margins using fluorescent marker seeds. *Am J Nucl Med Mol Imaging*. 2012; 2:151–62. [PubMed: 23133810]
16. Dayton PA, Rychak JJ. Molecular ultrasound imaging using microbubble contrast agents. *Front Biosci*. 2007; 12:5124–42. [PubMed: 17569635]
17. Nolting DD, Nickels ML, Guo N, Pham W. Molecular imaging probe development: a chemistry perspective. *Am J Nucl Med Mol Imaging*. 2012; 2:273–306. [PubMed: 22943038]
18. Thorek D, Robertson R, Bacchus WA, et al. Cerenkov imaging - a new modality for molecular imaging. *Am J Nucl Med Mol Imaging*. 2012; 2:163–73. [PubMed: 23133811]
19. Wang RE, Niu Y, Wu H, Amin MN, Cai J. Development of NGR peptide-based agents for tumor imaging. *Am J Nucl Med Mol Imaging*. 2011; 1:36–46. [PubMed: 23133793]
20. Zeman MN, Scott PJ. Current imaging strategies in rheumatoid arthritis. *Am J Nucl Med Mol Imaging*. 2012; 2:174–220. [PubMed: 23133812]
21. Yu MK, Jeong YY, Park J, et al. Drug-loaded superparamagnetic iron oxide nanoparticles for combined cancer imaging and therapy in vivo. *Angew Chem Int Edit*. 2008; 47:5362–5.
22. Amstad E, Zurcher S, Mashaghi A, et al. Surface Functionalization of Single Superparamagnetic Iron Oxide Nanoparticles for Targeted Magnetic Resonance Imaging. *Small*. 2009; 5:1334–42. [PubMed: 19242944]
23. Chaugule RS, Purushotham S, Ramanujan RV. Magnetic Nanoparticles as Contrast Agents for Magnetic Resonance Imaging. *P Natl a Sci India A*. 2012; 82:257–68.
24. Dubertret B, Skourides P, Norris DJ, et al. In vivo imaging of quantum dots encapsulated in phospholipid micelles. *Science*. 2002; 298:1759–62. [PubMed: 12459582]
25. Gao XH, Cui YY, Levenson RM, Chung LWK, Nie SM. In vivo cancer targeting and imaging with semiconductor quantum dots. *Nat Biotechnol*. 2004; 22:969–76. [PubMed: 15258594]
26. Gao JH, Chen K, Xie RG, et al. Ultrasmall Near-Infrared Non-cadmium Quantum Dots for in vivo Tumor Imaging. *Small*. 2010; 6:256–61. [PubMed: 19911392]
27. Cai W, Hong H. a “nutshell”: intrinsically radio-labeled quantum dots. *Am J Nucl Med Mol Imaging*. 2012; 2:136–40. [PubMed: 23133808]
28. Sun M, Hoffman D, Sundaresan G, et al. Synthesis and characterization of intrinsically radiolabeled quantum dots for bimodal detection. *Am J Nucl Med Mol Imaging*. 2012; 2:122–35. [PubMed: 23133807]
29. Shi DL, Guo Y, Dong ZY, et al. Quantum-dot-activated luminescent carbon nanotubes via a nano scale surface functionalization for in vivo imaging. *Adv Mater*. 2007; 19:4033–7.
30. Robinson JT, Hong GS, Liang YY, et al. In Vivo Fluorescence Imaging in the Second Near-Infrared Window with Long Circulating Carbon Nanotubes Capable of Ultrahigh Tumor Uptake. *J Am Chem Soc*. 2012; 134:10664–9. [PubMed: 22667448]
31. Tao HQ, Yang K, Ma Z, et al. In Vivo NIR Fluorescence Imaging, Biodistribution, and Toxicology of Photoluminescent Carbon Dots Produced from Carbon Nanotubes and Graphite. *Small*. 2012; 8:281–90.
32. Kim D, Park S, Lee JH, Jeong YY, Jon S. Antibiofouling polymer-coated gold nanoparticles as a contrast agent for in vivo x-ray computed tomography imaging. *J Am Chem Soc*. 2007; 129:7661–5. [PubMed: 17530850]

33. Lee S, Cha EJ, Park K, et al. A near-infrared-fluorescence-quenched gold-nanoparticle imaging probe for in vivo drug screening and protease activity determination. *Angew Chem Int Edit*. 2008; 47:2804–7.
34. Yigit MV, Medarova Z. In vivo and ex vivo applications of gold nanoparticles for biomedical SERS imaging. *Am J Nucl Med Mol Imaging*. 2012; 2:232–41. [PubMed: 23133814]
35. Hong H, Yang K, Zhang Y, et al. In Vivo Targeting and Imaging of Tumor Vasculature with Radiolabeled, Antibody-Conjugated Nanographene. *ACS Nano*. 2012; 6:2361–70. [PubMed: 22339280]
36. Hong H, Zhang Y, Engle JW, et al. In vivo targeting and positron emission tomography imaging of tumor vasculature with <sup>66</sup>Ga-labeled nano-graphene. *Biomaterials*. 2012; 33:4147–56. [PubMed: 22386918]
37. Gollavelli G, Ling YC. Multi-functional graphene as an in vitro and in vivo imaging probe. *Biomaterials*. 2012; 33:2532–45. [PubMed: 22206596]
38. Resch-Genger U, Grabolle M, Cavaliere-Jaricot S, Nitschke R, Nann T. Quantum dots versus organic dyes as fluorescent labels. *Nat Methods*. 2008; 5:763–75. [PubMed: 18756197]
39. Efros AL, Efros AL. Interband Absorption of Light in a Semiconductor Sphere. *Sov Phys Semicond+*. 1982; 16:772–5.
40. Brus L. Electronic Wave-Functions in Semiconductor Clusters - Experiment and Theory. *J Phys Chem-US*. 1986; 90:2555–60.
41. Wang Y, Herron N. Nanometer-Sized Semiconductor Clusters - Materials Synthesis, Quantum Size Effects, and Photophysical Properties. *J Phys Chem-US*. 1991; 95:525–32.
42. Alivisatos AP. Semiconductor clusters, nanocrystals, and quantum dots. *Science*. 1996; 271:933–7.
43. Michalet X, Pinaud FF, Bentolila LA, et al. Quantum dots for live cells, in vivo imaging, and diagnostics. *Science*. 2005; 307:538–44. [PubMed: 15681376]
44. Delehanty JB, Mattoussi H, Medintz IL. Delivering quantum dots into cells: strategies, progress and remaining issues. *Anal Bioanal Chem*. 2009; 393:1091–105. [PubMed: 18836855]
45. Murphy JE, Beard MC, Norman AG, et al. PbTe colloidal nanocrystals: Synthesis, characterization, and multiple exciton generation. *J Am Chem Soc*. 2006; 128:3241–7. [PubMed: 16522105]
46. Kang H, Clarke ML, Lacerda SHD, et al. Multimodal optical studies of single and clustered colloidal quantum dots for the long-term optical property evaluation of quantum dot-based molecular imaging phantoms. *Biomed Opt Express*. 2012; 3:1312–25. [PubMed: 22741078]
47. Taylor A, Wilson KM, Murray P, Fernig DG, Levy R. Long-term tracking of cells using inorganic nanoparticles as contrast agents: are we there yet? *Chem Soc Rev*. 2012; 41:2707–17. [PubMed: 22362426]
48. Qu Y, Li W, Zhou YL, et al. Full Assessment of Fate and Physiological Behavior of Quantum Dots Utilizing *Caenorhabditis elegans* as a Model Organism. *Nano Lett*. 2011; 11:3174–83. [PubMed: 21721562]
49. Hauck TS, Anderson RE, Fischer HC, Newbigging S, Chan WCW. In vivo Quantum-Dot Toxicity Assessment. *Small*. 2010; 6:138–44. [PubMed: 19743433]
50. Zhang W, Lin KF, Miao YN, et al. Toxicity assessment of zebrafish following exposure to CdTe QDs. *J Hazard Mater*. 2012; 213:413–20. [PubMed: 22381373]
51. Ye L, Yong KT, Liu LW, et al. A pilot study in non-human primates shows no adverse response to intravenous injection of quantum dots. *Nat Nanotechnol*. 2012; 7:453–8. [PubMed: 22609691]
52. Su YY, Peng F, Jiang ZY, et al. In vivo distribution, pharmacokinetics, and toxicity of aqueous synthesized cadmium-containing quantum dots. *Biomaterials*. 2011; 32:5855–62. [PubMed: 21601920]
53. Liu YS, Sun YH, Vernier PT, et al. pH-sensitive photoluminescence of CdSe/ZnSe/ZnS quantum dots in human ovarian cancer cells. *J Phys Chem C*. 2007; 111:2872–8.
54. Loginova YF, Dezhurov SV, Zherdeva VV, et al. Biodistribution and stability of CdSe core quantum dots in mouse digestive tract following per os administration: Advantages of double polymer/silica coated nanocrystals. *Biochem Bioph Res Co*. 2012; 419:54–9.

55. Nicolas J, Brambilla D, Carion O, et al. Quantum dot-loaded PEGylated poly(alkyl cyanoacrylate) nanoparticles for in vitro and in vivo imaging. *Soft Matter*. 2011; 7:6187–93.
56. Jayagopal A, Russ PK, Haselton FR. Surface engineering of quantum dots for in vivo vascular Imaging. *Bioconjugate Chem*. 2007; 18:1424–33.
57. Talapin DV, Haubold S, Rogach AL, et al. A novel organometallic synthesis of highly luminescent CdTe nanocrystals. *J Phys Chem B*. 2001; 105:2260–3.
58. Qu LH, Peng ZA, Peng XG. Alternative routes toward high quality CdSe nanocrystals. *Nano Lett*. 2001; 1:333–7.
59. Smith AM, Ruan G, Rhyner MN, Nie SM. Engineering luminescent quantum dots for In vivo molecular and cellular imaging. *Ann Biomed Eng*. 2006; 34:3–14. [PubMed: 16450199]
60. Peng ZA, Peng XG. Formation of high-quality CdTe, CdSe, and CdS nanocrystals using CdO as precursor. *J Am Chem Soc*. 2001; 123:183–4. [PubMed: 11273619]
61. Rogach AL, Katsikas L, Kornowski A, et al. Synthesis and characterization of thiol-stabilized CdTe nanocrystals. *Ber Bunsen Phys Chem*. 1996; 100:1772–8.
62. Zou L, Gu ZY, Zhang N, et al. Ultrafast synthesis of highly luminescent green- to near infrared-emitting CdTe nanocrystals in aqueous phase. *J Mater Chem*. 2008; 18:2807–15.
63. Kalasad MN, Rabinal AK, Mulimani BG. Ambient Synthesis and Characterization of High-Quality CdSe Quantum Dots by an Aqueous Route. *Langmuir*. 2009; 25:12729–35. [PubMed: 19711933]
64. Law WC, Yong KT, Roy I, et al. Aqueous-Phase Synthesis of Highly Luminescent CdTe/ZnTe Core/Shell Quantum Dots Optimized for Targeted Bioimaging. *Small*. 2009; 5:1302–10. [PubMed: 19242947]
65. Zhu Y, Li Z, Chen M, et al. One-pot preparation of highly fluorescent cadmium telluride/cadmium sulfide quantum dots under neutral-pH condition for biological applications. *J Colloid Interf Sci*. 2013; 390:3–10.
66. Bao HB, Gong YJ, Li Z, Gao MY. Enhancement effect of illumination on the photoluminescence of water-soluble CdTe nanocrystals: Toward highly fluorescent CdTe/CdS core-shell structure. *Chem Mater*. 2004; 16:3853–9.
67. Zhang H, Wang LP, Xiong HM, et al. Hydrothermal synthesis for high-quality CdTe nanocrystals. *Adv Mater*. 2003; 15:1712–5.
68. Jian DL, Gao QM. Synthesis of CdS nanocrystals and Au/CdS nanocomposites through ultrasound activation liquid-liquid two-phase approach at room temperature. *Chem Eng J*. 2006; 121:9–16.
69. Duan JL, Song LX, Zhan JH. One-Pot Synthesis of Highly Luminescent CdTe Quantum Dots by Microwave Irradiation Reduction and Their Hg<sup>2+</sup>-Sensitive Properties. *Nano Res*. 2009; 2:61–8.
70. Talapin DV, Mekis I, Gotzinger S, et al. CdSe/CdS/ZnS and CdSe/ZnSe/ZnS core-shell-shell nanocrystals. *J Phys Chem B*. 2004; 108:18826–31.
71. Marchi-Artzner V, Dif A, Henry E, et al. Interaction between water-soluble peptidic CdSe/ZnS nanocrystals and membranes: Formation of hybrid vesicles and condensed lamellar phases. *J Am Chem Soc*. 2008; 130:8289–96. [PubMed: 18529051]
72. Kirchner C, Liedl T, Kudera S, et al. Cytotoxicity of colloidal CdSe and CdSe/ZnS nanoparticles. *Nano Lett*. 2005; 5:331–8. [PubMed: 15794621]
73. Akerman ME, Chan WCW, Laakkonen P, Bhatia SN, Ruoslahti E. Nanocrystal targeting in vivo. *Natl Acad Sci USA*. 2002; 99:12617–21.
74. Yu XF, Chen LD, Li KY, et al. Immunofluorescence detection with quantum dot bioconjugates for hepatoma in vivo. *J Biomed Opt*. 2007; 12:014008. [PubMed: 17343483]
75. Diagaradjane P, Orenstein-Cardona JM, Colon-Casasnovas NE, et al. Imaging epidermal growth factor receptor expression in vivo: Pharmacokinetic and biodistribution characterization of a bioconjugated quantum dot nanoprobe. *Clin Cancer Res*. 2008; 14:731–41. [PubMed: 18245533]
76. Yang LL, Mao H, Wang YA, et al. Single Chain Epidermal Growth Factor Receptor Antibody Conjugated Nanoparticles for in vivo Tumor Targeting and Imaging. *Small*. 2009; 5:235–43. [PubMed: 19089838]
77. Kato S, Itoh K, Yaoi T, et al. Organ distribution of quantum dots after intraperitoneal administration, with special reference to area-specific distribution in the brain. *Nanotechnology*. 2010; 21:335103. [PubMed: 20660952]



78. Lu RM, Chang YL, Chen MS, Wu HC. Single chain anti-c-Met antibody conjugated nanoparticles for in vivo tumor-targeted imaging and drug delivery. *Biomaterials*. 2011; 32:3265–74. [PubMed: 21306768]
79. Mukthavaram R, Wrasidlo W, Hall D, Kesari S, Makale M. Assembly and Targeting of Liposomal Nanoparticles Encapsulating Quantum Dots. *Bioconjugate Chem*. 2011; 22:1638–44.
80. Wang WW, Cheng D, Gong FM, Miao XM, Shuai XT. Design of Multifunctional Micelle for Tumor-Targeted Intracellular Drug Release and Fluorescent Imaging. *Adv Mater*. 2012; 24:115–20. [PubMed: 22143956]
81. Cai WB, Shin DW, Chen K, et al. Peptide-labeled near-infrared quantum dots for imaging tumor vasculature in living subjects. *Nano Lett*. 2006; 6:669–76. [PubMed: 16608262]
82. Ding H, Yong KT, Law WC, et al. Non-invasive tumor detection in small animals using novel functional Pluronic nanomicelles conjugated with anti-mesothelin antibody. *Nanoscale*. 2011; 3:1813–22. [PubMed: 21365120]
83. Liu LW, Yong KT, Roy I, et al. Bioconjugated Pluronic Triblock-Copolymer Micelle-Encapsulated Quantum Dots for Targeted Imaging of Cancer: In Vitro and In Vivo Studies. *Theranostics*. 2012; 2:705–13. [PubMed: 22896772]
84. Cao J, Zhu HY, Deng DW, et al. In vivo NIR imaging with PbS quantum dots entrapped in biodegradable micelles. *J Biomed Mater Res A*. 2012; 100A:958–68. [PubMed: 22275223]
85. Chen HY, Li L, Cui SS, et al. Folate Conjugated CdHgTe Quantum Dots with High Targeting Affinity and Sensitivity for In vivo Early Tumor Diagnosis. *J Fluoresc*. 2011; 21:793–801. [PubMed: 21113651]
86. Han SH, Mu Y, Zhu QY, et al. Au:CdHgTe quantum dots for in vivo tumor-targeted multispectral fluorescence imaging. *Anal Bioanal Chem*. 2012; 403:1343–52. [PubMed: 22447216]
87. He Y, Zhong YL, Su YY, et al. Water-Dispersed Near-Infrared-Emitting Quantum Dots of Ultrasmall Sizes for In Vitro and In Vivo Imaging. *Angew Chem Int Edit*. 2011; 50:5694–7.
88. Gao JH, Chen K, Xie RG, et al. In Vivo Tumor-Targeted Fluorescence Imaging Using Near-Infrared Non-Cadmium Quantum Dots. *Bioconjugate Chem*. 2010; 21:604–9.
89. Deng DW, Chen YQ, Cao J, et al. High-Quality CuInS<sub>2</sub>/ZnS Quantum Dots for In vitro and In vivo Bioimaging. *Chem Mater*. 2012; 24:3029–37.
90. Li L, Daou TJ, Texier I, et al. Highly Luminescent CuInS<sub>2</sub>/ZnS Core/Shell Nanocrystals: Cadmium-Free Quantum Dots for In Vivo Imaging. *Chem Mater*. 2009; 21:2422–9.
91. Cassette E, Pons T, Bouet C, et al. Synthesis and Characterization of Near-Infrared Cu-In-Se/ZnS Core/Shell Quantum Dots for In vivo Imaging. *Chem Mater*. 2010; 22:6117–24.
92. Erogbogbo F, Yong KT, Roy I, et al. In Vivo Targeted Cancer Imaging, Sentinel Lymph Node Mapping and Multi-Channel Imaging with Biocompatible Silicon Nanocrystals. *ACS Nano*. 2011; 5:413–23. [PubMed: 21138323]
93. Cao L, Wang X, Mezziani MJ, et al. Carbon dots for multiphoton bioimaging. *J Am Chem Soc*. 2007; 129:11318–9. [PubMed: 17722926]
94. Sun YP, Zhou B, Lin Y, et al. Quantum-sized carbon dots for bright and colorful photoluminescence. *J Am Chem Soc*. 2006; 128:7756–7. [PubMed: 16771487]
95. Zhou JG, Booker C, Li RY, et al. An electrochemical avenue to blue luminescent nanocrystals from multiwalled carbon nanotubes (MWCNTs). *J Am Chem Soc*. 2007; 129:744–5. [PubMed: 17243794]
96. Yang ST, Cao L, Luo PGJ, et al. Carbon Dots for Optical Imaging in Vivo. *J Am Chem Soc*. 2009; 131:11308–9. [PubMed: 19722643]
97. All-Jamal WT, Al-Jamal KT, Tian B, et al. Tumor Targeting of Functionalized Quantum Dot-Liposome Hybrids by Intravenous Administration. *Mol Pharmaceut*. 2009; 6:520–30.
98. Schipper ML, Iyer G, Koh AL, et al. Particle Size, Surface Coating, and PEGylation Influence the Biodistribution of Quantum Dots in Living Mice. *Small*. 2009; 5:126–34. [PubMed: 19051182]
99. Zintchenko A, Susha AS, Concia M, et al. Drug Nanocarriers Labeled With Near-infrared-emitting Quantum Dots (Quantoplexes): Imaging Fast Dynamics of Distribution in Living Animals. *Mol Ther*. 2009; 17:1849–56. [PubMed: 19707184]

100. Nurunnabi M, Cho KJ, Choi JS, Huh KM, Lee YH. Targeted near-IR QDs-loaded micelles for cancer therapy and imaging. *Biomaterials*. 2010; 31:5436–44. [PubMed: 20409581]
101. Kim JS, Cho KJ, Tran TH, et al. In vivo NIR imaging with CdTe/CdSe quantum dots entrapped in PLGA nanospheres. *J Colloid Interf Sci*. 2011; 353:363–71.
102. Wen CJ, Zhang LW, Al-Suwayeh SA, Yen TC, Fang JY. Theranostic liposomes loaded with quantum dots and apomorphine for brain targeting and bioimaging. *Int J Nanomed*. 2012; 7:1599–611.
103. Bruchez M, Moronne M, Gin P, Weiss S, Alivisatos AP. Semiconductor nanocrystals as fluorescent biological labels. *Science*. 1998; 281:2013–6. [PubMed: 9748157]
104. Szabo DV, Vollath D. Nanocomposites from coated nanoparticles. *Adv Mater*. 1999; 11:1313–6.
105. Derfus AM, Chan WCW, Bhatia SN. Probing the cytotoxicity of semiconductor quantum dots. *Nano Lett*. 2004; 4:11–8.
106. Chen Z, Chen H, Meng H, et al. Bio-distribution and metabolic paths of silica coated CdSe quantum dots. *Toxicol Appl Pharm*. 2008; 230:364–71.
107. Ma N, Marshall AF, Gambhir SS, Rao JH. Facile Synthesis, Silanization, and Biodistribution of Biocompatible Quantum Dots. *Small*. 2010; 6:1520–8. [PubMed: 20564726]
108. Curnis F, Sacchi A, Gasparri A, et al. Isoaspartate-glycine-arginine: A new tumor vasculature-targeting motif. *Cancer Res*. 2008; 68:7073–82. [PubMed: 18757422]
109. Goldman ER, Balighian ED, Mattoussi H, et al. Avidin: A natural bridge for quantum dot-antibody conjugates. *J Am Chem Soc*. 2002; 124:6378–82. [PubMed: 12033868]
110. Park J, Nam J, Won N, et al. Compact and Stable Quantum Dots with Positive, Negative, or Zwitterionic Surface: Specific Cell Interactions and Non-Specific Adsorptions by the Surface Charges. *Adv Funct Mater*. 2011; 21:1558–66.
111. Muro E, Fragola A, Pons T, et al. Comparing Intracellular Stability and Targeting of Sulfbetaine Quantum Dots with Other Surface Chemistries in Live Cells. *Small*. 2012; 8:1029–37. [PubMed: 22378567]
112. Howarth M, Liu WH, Puthenveetil S, et al. Monovalent, reduced-size quantum dots for imaging receptors on living cells. *Nat Methods*. 2008; 5:397–9. [PubMed: 18425138]
113. Hua XF, Liu TC, Cao YC, et al. Characterization of the coupling of quantum dots and immunoglobulin antibodies. *Anal Bioanal Chem*. 2006; 386:1665–71. [PubMed: 17033770]
114. Wu XY, Liu HJ, Liu JQ, et al. Immunofluorescent labeling of cancer marker Her2 and other cellular targets with semiconductor quantum dots. *Nat Biotechnol*. 2003; 21:41–6. [PubMed: 12459735]
115. Maldiney T, Kaikkonen MU, Seguin J, et al. In Vitro Targeting of Avidin-Expressing Glioma Cells with Biotinylated Persistent Luminescence Nanoparticles. *Bioconjugate Chem*. 2012; 23:472–8.
116. Chen L, Zhang XW, Zhou GH, et al. Simultaneous Determination of Human Enterovirus 71 and Coxsackievirus B3 by Dual-Color Quantum Dots and Homogeneous Immunoassay. *Anal Chem*. 2012; 84:3200–7. [PubMed: 22390751]
117. Allen PM, Liu WH, Chauhan VP, et al. InAs(ZnCdS) Quantum Dots Optimized for Biological Imaging in the Near-Infrared. *J Am Chem Soc*. 2010; 132:470–1. [PubMed: 20025222]
118. Bae PK, Kim KN, Lee SJ, et al. The modification of quantum dot probes used for the targeted imaging of his-tagged fusion proteins. *Biomaterials*. 2009; 30:836–42. [PubMed: 19027151]
119. Park HY, Kim K, Hong S, et al. Compact and Versatile Nickel-Nitrilotriacetate-Modified Quantum Dots for Protein Imaging and Forster Resonance Energy Transfer Based Assay. *Langmuir*. 2010; 26:7327–33. [PubMed: 20030352]
120. Susumu K, Medintz IL, Delehanty JB, Boeneman K, Mattoussi H. Modification of Poly(ethylene glycol)-Capped Quantum Dots with Nickel Nitrilotriacetic Acid and Self-Assembly with Histidine-Tagged Proteins. *J Phys Chem C*. 2010; 114:13526–31.
121. Bhang SH, Won N, Lee TJ, et al. Hyaluronic Acid-Quantum Dot Conjugates for In Vivo Lymphatic Vessel Imaging. *ACS Nano*. 2009; 3:1389–98. [PubMed: 19476339]

122. Yu HW, Kim IS, Niessner R, Knopp D. Multiplex competitive microbead-based flow cytometric immunoassay using quantum dot fluorescent labels. *Anal Chim Acta*. 2012; 750:191–8. [PubMed: 23062440]
123. Liou JS, Liu BR, Martin AL, et al. Protein transduction in human cells is enhanced by cell-penetrating peptides fused with an endosomolytic HA2 sequence. *Peptides*. 2012; 37:273–84. [PubMed: 22898256]
124. Zhang Y, So MK, Loening AM, et al. HaloTag protein-mediated site-specific conjugation of bioluminescent proteins to quantum dots. *Angew Chem Int Ed Engl*. 2006; 45:4936–40. [PubMed: 16807952]
125. Charalambous A, Antoniadis I, Christodoulou N, Skourides PA. Split-Inteins for Simultaneous, site-specific conjugation of Quantum Dots to multiple protein targets In vivo. *J Nanobiotechnol*. 2011; 9:37.
126. Wu Y, Zhang W, Li J, Zhang Y. Optical imaging of tumor microenvironment. *Am J Nucl Med Mol Imaging*. 2013; 3:1–15. [PubMed: 23342297]
127. Wong AW, Ormsby E, Zhang H, et al. A comparison of image contrast with  $^{64}\text{Cu}$ -labeled long circulating liposomes and  $^{18}\text{F}$ -FDG in a murine model of mammary carcinoma. *Am J Nucl Med Mol Imaging*. 2013; 3:32–43. [PubMed: 23342299]
128. Ballou B, Lagerholm BC, Ernst LA, Bruchez MP, Waggoner AS. Noninvasive imaging of quantum dots in mice. *Bioconjugate Chem*. 2004; 15:79–86.
129. Choi HS, Liu W, Misra P, et al. Renal clearance of quantum dots. *Nat Biotechnol*. 2007; 25:1165–70. [PubMed: 17891134]
130. Lee HA, Imran M, Monteiro-Riviere NA, et al. Biodistribution of quantum dot nanoparticles in perfused skin: Evidence of coating dependency and periodicity in arterial extraction. *Nano Lett*. 2007; 7:2865–70. [PubMed: 17685663]
131. Chen HY, Cui SS, Tu ZZ, Gu YQ, Chi XM. In vivo Monitoring of Organ-Selective Distribution of CdHgTe/SiO<sub>2</sub> Nanoparticles in Mouse Model. *J Fluoresc*. 2012; 22:699–706. [PubMed: 22083240]
132. Praetner M, Rehberg M, Bihari P, et al. The contribution of the capillary endothelium to blood clearance and tissue deposition of anionic quantum dots in vivo. *Biomaterials*. 2010; 31:6692–700. [PubMed: 20619783]
133. Cai WB, Chen XY. Preparation of peptide-conjugated quantum dots for tumor vasculature-targeted imaging. *Nat Protoc*. 2008; 3:89–96. [PubMed: 18193025]
134. Yong KT, Hu R, Roy I, et al. Tumor Targeting and Imaging in Live Animals with Functionalized Semiconductor Quantum Rods. *ACS Appl Mater Inter*. 2009; 1:710–9.
135. Cai W, Niu G, Chen X. Imaging of integrins as biomarkers for tumor angiogenesis. *Curr Pharm Des*. 2008; 14:2943–73. [PubMed: 18991712]
136. Cai W, Chen X. Multimodality molecular imaging of tumor angiogenesis. *J Nucl Med*. 2008; 49(Suppl 2):113S–28S. [PubMed: 18523069]
137. Yong KT. Biophotonics and Biotechnology in Pancreatic Cancer: Cyclic RGD-Peptide-Conjugated Type II Quantum Dots for in vivo Imaging. *Pancreatol*. 2010; 10:553–64. [PubMed: 20975319]
138. Yong KT, Roy I, Law WC, Hu R. Synthesis of cRGD-peptide conjugated near-infrared CdTe/ZnSe core-shell quantum dots for in vivo cancer targeting and imaging. *Chem Commun*. 2010; 46:7136–8.
139. Li Y, Li Z, Wang XH, et al. In Vivo Cancer Targeting and Imaging-Guided Surgery with Near Infrared-Emitting Quantum Dot Bioconjugates. *Theranostics*. 2012; 2:769–76. [PubMed: 22916076]
140. Gao JH, Chen K, Luong R, et al. A Novel Clinically Translatable Fluorescent Nanoparticle for Targeted Molecular Imaging of Tumors in Living Subjects. *Nano Lett*. 2012; 12:281–6. [PubMed: 22172022]
141. Tada H, Higuchi H, Wanatabe TM, Ohuchi N. In vivo real-time tracking of single quantum dots conjugated with monoclonal anti-HER2 antibody in tumors of mice. *Cancer Res*. 2007; 67:1138–44. [PubMed: 17283148]

142. Zhang Y, Cai W. Molecular imaging of insulin-like growth factor 1 receptor in cancer. *Am J Nucl Med Mol Imaging*. 2012; 2:248–59. [PubMed: 23066521]
143. Zhang H, Zeng X, Li Q, et al. Fluorescent tumour imaging of type I IGF receptor in vivo: comparison of antibody-conjugated quantum dots and small-molecule fluorophore. *Brit J Cancer*. 2009; 101:71–9. [PubMed: 19491901]
144. Hassan R, Ho M. Mesothelin targeted cancer immunotherapy. *Eur J Cancer*. 2008; 44:46–53. [PubMed: 17945478]
145. Baselga J. Targeting tyrosine kinases in cancer: The second wave. *Science*. 2006; 312:1175–8. [PubMed: 16728632]
146. Cai W, Niu G, Chen X. Multimodality imaging of the HER-kinase axis in cancer. *Eur J Nucl Med Mol Imaging*. 2008; 35:186–208. [PubMed: 17846765]
147. Rogers SJ, Harrington KJ, Rhys-Evans P, Charoenrat PO, Eccles SA. Biological significance of c-erbB family oncogenes in head and neck cancer. *Cancer Metast Rev*. 2005; 24:47–69.
148. Kalyankrishna S, Grandis JR. Epidermal growth factor receptor biology in head and neck cancer. *J Clin Oncol*. 2006; 24:2666–72. [PubMed: 16763281]
149. Yang K, Zhang FJ, Tang H, et al. In-vivo imaging of oral squamous cell carcinoma by EGFR monoclonal antibody conjugated near-infrared quantum dots in mice. *Int J Nanomed*. 2011; 6:1739–45.
150. Zhou Y, Daryl C, Zou H, et al. Impact of single-chain fv antibody fragment affinity on nanoparticle targeting of epidermal growth factor receptor-expressing tumor cells. *J Mol Biol*. 2007; 371:934–47. [PubMed: 17602702]
151. Lee AS. GRP78 induction in cancer: Therapeutic and prognostic implications. *Cancer Res*. 2007; 67:3496–9. [PubMed: 17440054]
152. Xu WM, Liu LZ, Brown NJ, Christian S, Hornby D. Quantum Dot- Conjugated Anti-GRP78 scFv Inhibits Cancer Growth in Mice. *Molecules*. 2012; 17:796–808. [PubMed: 22249409]
153. Jung KH, Park BH, Hong SS. Progress in cancer therapy targeting c-Met signaling pathway. *Arch Pharm Res*. 2012; 35:595–604. [PubMed: 22553051]
154. Liu X, Yao W, Newton RC, Scherle PA. Targeting the c-MET signaling pathway for cancer therapy. *Expert Opin Investig Drugs*. 2008; 17:997–1011.
155. Jung KH, Choe YS, Paik JY, Lee KH. <sup>99m</sup>Tc-Hydrazinonicotinamide Epidermal Growth Factor-Polyethylene Glycol-Quantum Dot Imaging Allows Quantification of Breast Cancer Epidermal Growth Factor Receptor Expression and Monitors Receptor Downregulation in Response to Cetuximab Therapy. *J Nucl Med*. 2011; 52:1457–64. [PubMed: 21849406]
156. Zhang L, Chang RC, Chu LW, Mak HK. Current neuroimaging techniques in Alzheimer s disease and applications in animal models. *Am J Nucl Med Mol Imaging*. 2012; 2:386–404. [PubMed: 23133824]
157. Gao XL, Chen J, Chen JY, et al. Quantum Dots Bearing Lectin-Functionalized Nanoparticles as a Platform for In Vivo Brain Imaging. *Bioconjugate Chem*. 2008; 19:2189–95.
158. Gao XL, Tao WX, Lu W, et al. Lectin-conjugated PEG-PLA nanoparticles: Preparation and brain delivery after intranasal administration. *Biomaterials*. 2006; 27:3482–90. [PubMed: 16510178]
159. Hong H, Goel S, Zhang Y, Cai W. Molecular imaging with nucleic acid aptamers. *Curr Med Chem*. 2011; 18:4195–205. [PubMed: 21838686]
160. Zhang Y, Hong H, Cai W. Tumor-targeted drug delivery with aptamers. *Curr Med Chem*. 2011; 18:4185–94. [PubMed: 21838687]
161. Zhang J, Jia X, Lv XJ, Deng YL, Xie HY. Fluorescent quantum dot-labeled aptamer bioprobes specifically targeting mouse liver cancer cells. *Talanta*. 2010; 81:505–9. [PubMed: 20188954]
162. Cui ZQ, Ren Q, Wei HP, et al. Quantum dot-aptamer nanoprobe for recognizing and labeling influenza A virus particles. *Nanoscale*. 2011; 3:2454–7. [PubMed: 21509395]
163. Hu D, Zhang P, Gong P, et al. A fast synthesis of near-infrared emitting CdTe/CdSe quantum dots with small hydrodynamic diameter for in vivo imaging probes. *Nanoscale*. 2011; 3:4724–32. [PubMed: 21989776]

164. Savla R, Taratula O, Garbuzenko O, Minko T. Tumor targeted quantum dot-mucin 1 aptamer-doxorubicin conjugate for imaging and treatment of cancer. *J Control Release*. 2011; 153:16–22. [PubMed: 21342659]
165. Segal EI, Low PS. Tumor detection using folate receptor-targeted imaging agents. *Cancer Metast Rev*. 2008; 27:655–64.
166. Chen LN, Wang J, Li WT, Han HY. Aqueous one-pot synthesis of bright and ultrasmall CdTe/CdS near-infrared-emitting quantum dots and their application for tumor targeting in vivo. *Chem Commun*. 2012; 48:4971–3.
167. Xue B, Deng DW, Cao J, et al. Synthesis of NAC capped near infrared-emitting CdTeS alloyed quantum dots and application for in vivo early tumor imaging. *Dalton T*. 2012; 41:4935–47.
168. Ossipov DA. Nanostructured hyaluronic acid-based materials for active delivery to cancer. *Expert Opin Drug Deliv*. 2010; 7:681–703. [PubMed: 20367530]
169. Kikkeri R, Lepenies B, Adibekian A, Laurino P, Seeberger PH. In Vitro Imaging and in Vivo Liver Targeting with Carbohydrate Capped Quantum Dots. *J Am Chem Soc*. 2009; 131:2110–2. [PubMed: 19199612]
170. Chakravarthy KV, Davidson BA, Helinski JD, et al. Doxorubicin-conjugated quantum dots to target alveolar macrophages and inflammation. *Nanomed-Nanotechnol*. 2011; 7:88–96.
171. Mulder WJM, Koole R, Brandwijk RJ, et al. Quantum dots with a paramagnetic coating as a bimodal molecular imaging probe. *Nano Lett*. 2006; 6:1–6. [PubMed: 16402777]
172. Cho HS, Dong Z, Pauletti GM, et al. Fluorescent, superparamagnetic nanospheres for drug storage, targeting, and imaging: a multifunctional nanocarrier system for cancer diagnosis and treatment. *ACS Nano*. 2010; 4:5398–404. [PubMed: 20707381]
173. Tan YF, Chandrasekharan P, Maity D, et al. Multimodal tumor imaging by iron oxides and quantum dots formulated in poly (lactic acid)-D-alpha-tocopheryl polyethylene glycol 1000 succinate nanoparticles. *Biomaterials*. 2011; 32:2969–78. [PubMed: 21257200]
174. Wang K, Ruan J, Qian QR, et al. BRCA1 monoclonal antibody conjugated fluorescent magnetic nanoparticles for in vivo targeted magnetofluorescent imaging of gastric cancer. *J Nanobiotechnol*. 2011; 9:23.
175. Ma Q, Nakane Y, Mori Y, et al. Multilayered, core/shell nanoprobe based on magnetic ferric oxide particles and quantum dots for multimodality imaging of breast cancer tumors. *Biomaterials*. 2012; 33:8486–94. [PubMed: 22906608]
176. Rudd JH, Hyafil F, Fayad ZA. Inflammation imaging in atherosclerosis. *Arterioscler Thromb Vasc Biol*. 2009; 29:1009–16. [PubMed: 19304673]
177. Temma T, Saji H. Radiolabelled probes for imaging of atherosclerotic plaques. *Am J Nucl Med Mol Imaging*. 2012; 2:432–47. [PubMed: 23145360]
178. Ding J, Wang Y, Ma M, et al. CT/fluorescence dual-modal nanoemulsion platform for investigating atherosclerotic plaques. *Biomaterials*. 2013; 34:209–16. [PubMed: 23069709]
179. Alauddin MM. Positron emission tomography (PET) imaging with <sup>18</sup>F-based radiotracers. *Am J Nucl Med Mol Imaging*. 2012; 2:55–76. [PubMed: 23133802]
180. Eary JF, Hawkins DS, Rodler ET, Conrad EU 3rd. <sup>18</sup>F-FDG PET in sarcoma treatment response imaging. *Am J Nucl Med Mol Imaging*. 2011; 1:47–53. [PubMed: 23133794]
181. Grassi I, Nanni C, Allegri V, et al. The clinical use of PET with <sup>11</sup>C-acetate. *Am J Nucl Med Mol Imaging*. 2012; 2:33–47. [PubMed: 23133801]
182. Vach W, Hoiland-Carlsen PF, Fischer BM, Gerke O, Weber W. How to study optimal timing of PET/CT for monitoring of cancer treatment. *Am J Nucl Med Mol Imaging*. 2011; 1:54–62. [PubMed: 23133795]
183. Cai WB, Chen K, Li ZB, Gambhir SS, Chen XY. Dual-function probe for PET and near-infrared fluorescence imaging of tumor vasculature. *J Nucl Med*. 2007; 48:1862–70. [PubMed: 17942800]
184. Chen K, Li ZB, Wang H, Cai WB, Chen XY. Dual-modality optical and positron emission tomography imaging of vascular endothelial growth factor receptor on tumor vasculature using quantum dots. *Eur J Nucl Med Mol Imaging*. 2008; 35:2235–44. [PubMed: 18566815]
185. Cai W, Chen X. Nanoplatforams for targeted molecular imaging in living subjects. *Small*. 2007; 3:1840–54. [PubMed: 17943716]

186. Cai W, Hsu AR, Li ZB, Chen X. Are quantum dots ready for *in vivo* imaging in human subjects? *Nanoscale Res Lett.* 2007; 2:265–81. [PubMed: 21394238]
187. Ho YP, Leong KW. Quantum dot-based theranostics. *Nanoscale.* 2010; 2:60–8. [PubMed: 20648364]
188. Kelkar SS, Reineke TM. Theranostics: combining imaging and therapy. *Bioconjug Chem.* 2011; 22:1879–903. [PubMed: 21830812]
189. Lee DY, Li KC. Molecular theranostics: a primer for the imaging professional. *AJR Am J Roentgenol.* 2011; 197:318–24. [PubMed: 21785076]

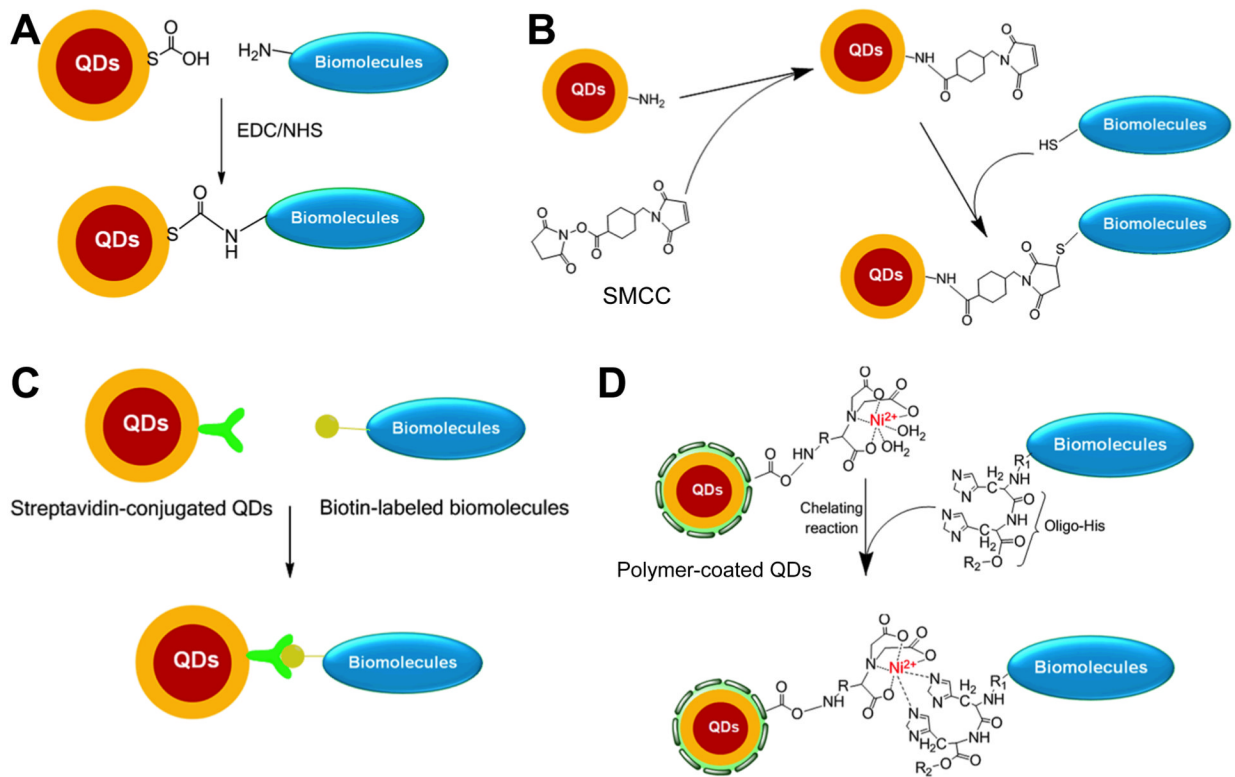


**Fig. (1).** Representative strategies for bioconjugation of QDs via EDC/NHS coupling (**A**), thiol-maleimide reaction (**B**), streptavidin-biotin binding (**C**), and interaction between Ni-NTA and histidine (**D**).

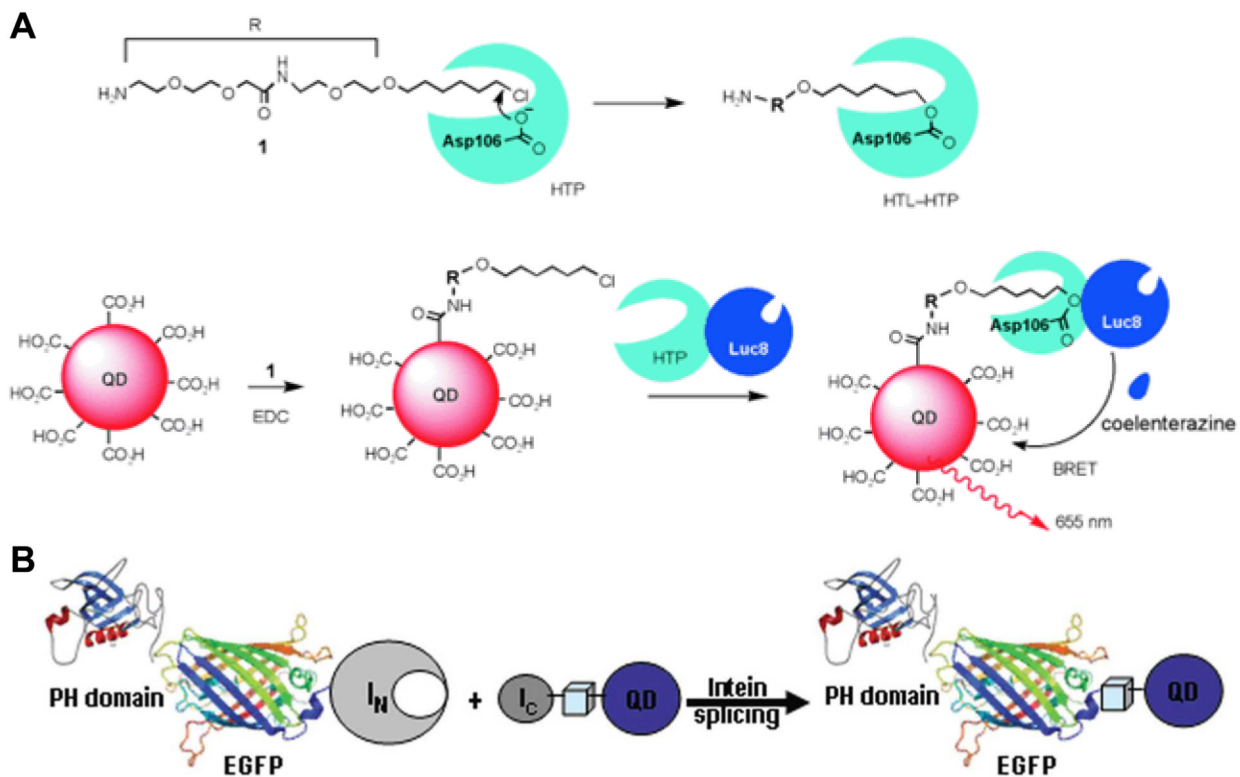


**Fig. (2).** (A) Modification of QDs through the use of HaloTag protein (HTP) and its ligand (HTL) for bioluminescence resonance energy transfer (BRET). (B) *In vivo* conjugation of QDs to representative proteins via intein-mediated protein splicing. Adapted from [124, 125].



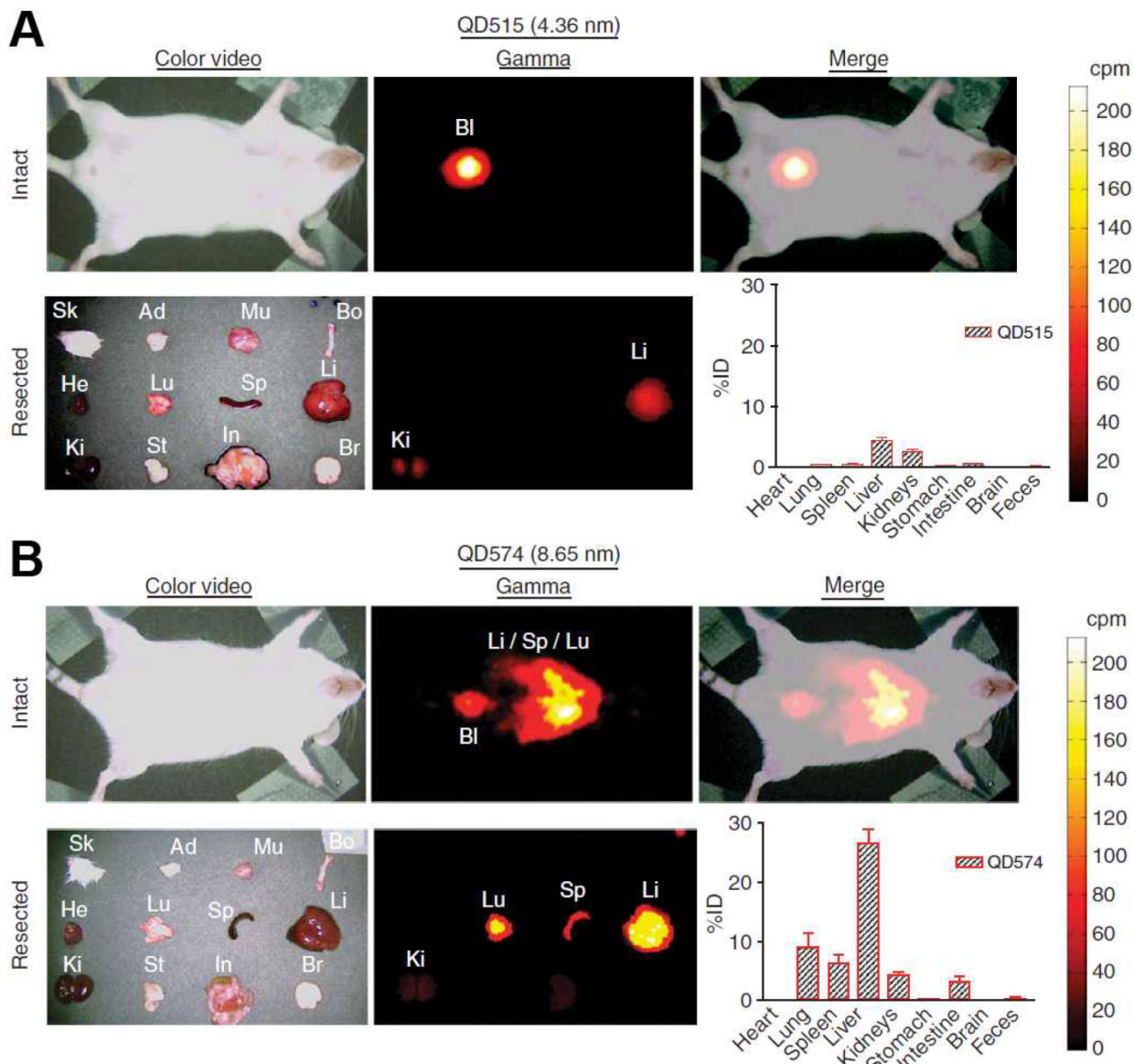


**Fig. (3).** QDs of different sizes exhibited different clearance pattern from mice after intravenous injection. **(A)** Renal clearance of QD515 which has a hydrodynamic diameter of 4.36 nm. **(B)** Poor clearance with high liver and lung uptake for QD574, which has a hydrodynamic diameter of 8.65 nm. Bl: bladder; Ki: kidney; Li: liver; Lu: lung; Sp: spleen. Adapted from [129].



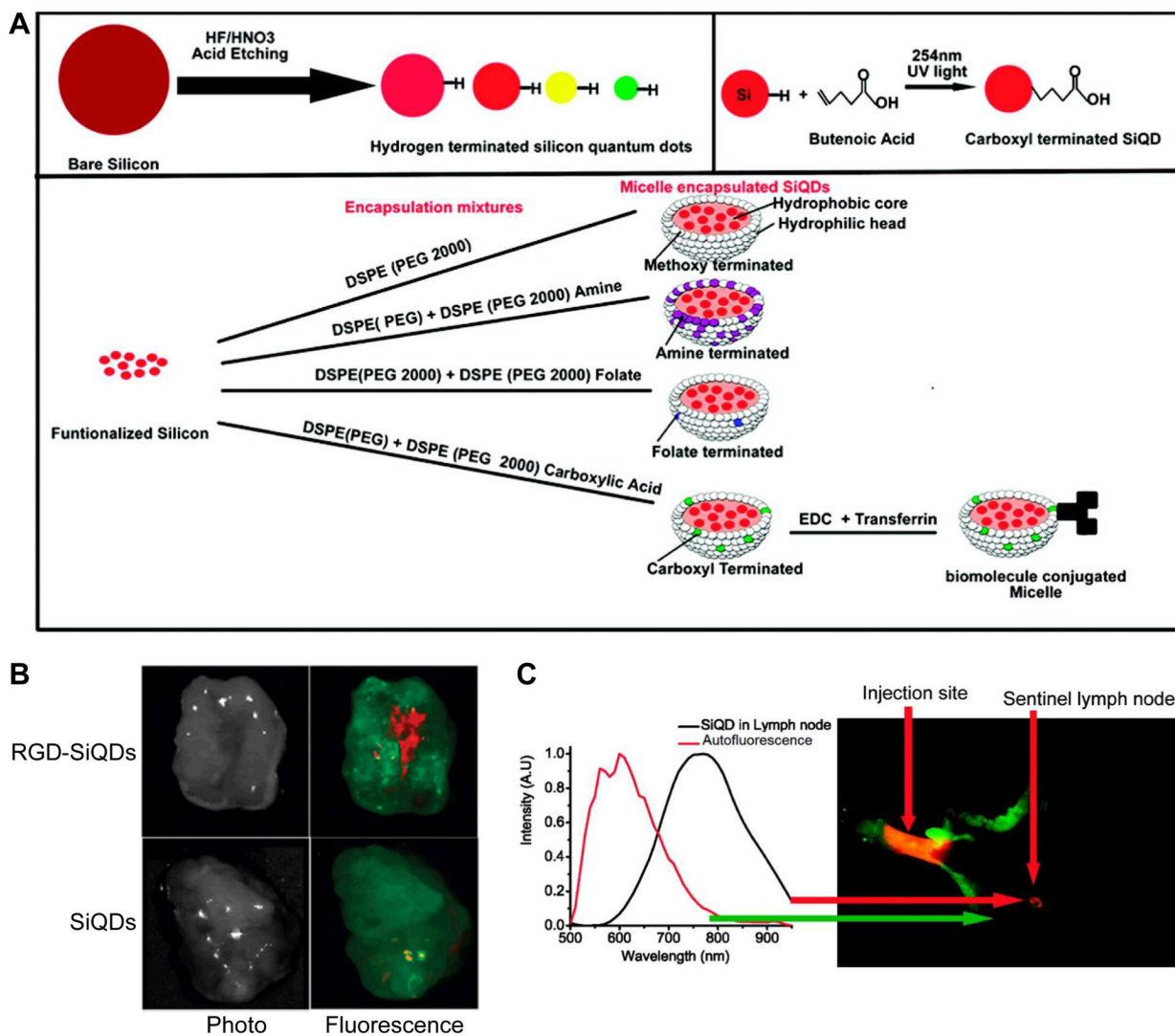


**Fig. (5).**

(A) Scheme for the synthesis and surface functionalization of SiQDs. (B) Tumor targeting of RGD-SiQDs and non-targeted SiQDs at 40 h post-injection based on *ex vivo* imaging. (C) Sentinel lymph node imaging captured the fluorescence of SiQDs in an axillary position. Red color indicates QD fluorescence and mouse autofluorescence is shown in green. Adapted from [92].

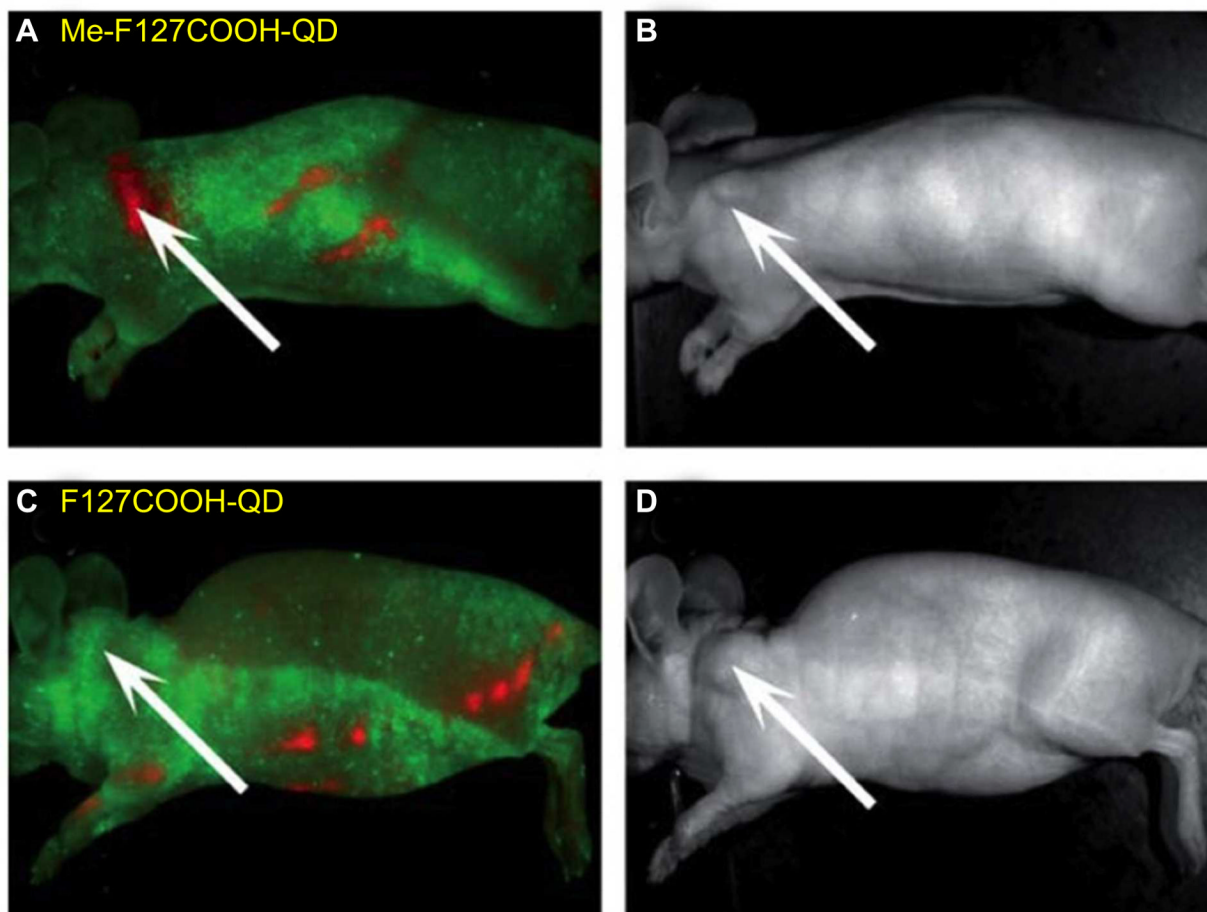


**Fig. (6).** Me-F127COOH-QD exhibited high tumor targeting efficiency (**A**) over non-targeted F127COOH-QD (**C**) in a human pancreatic cancer model. **B** and **D** are corresponding photos of mice in **A** and **C**. Me denotes an anti-methoselin antibody. Adapted from [82].

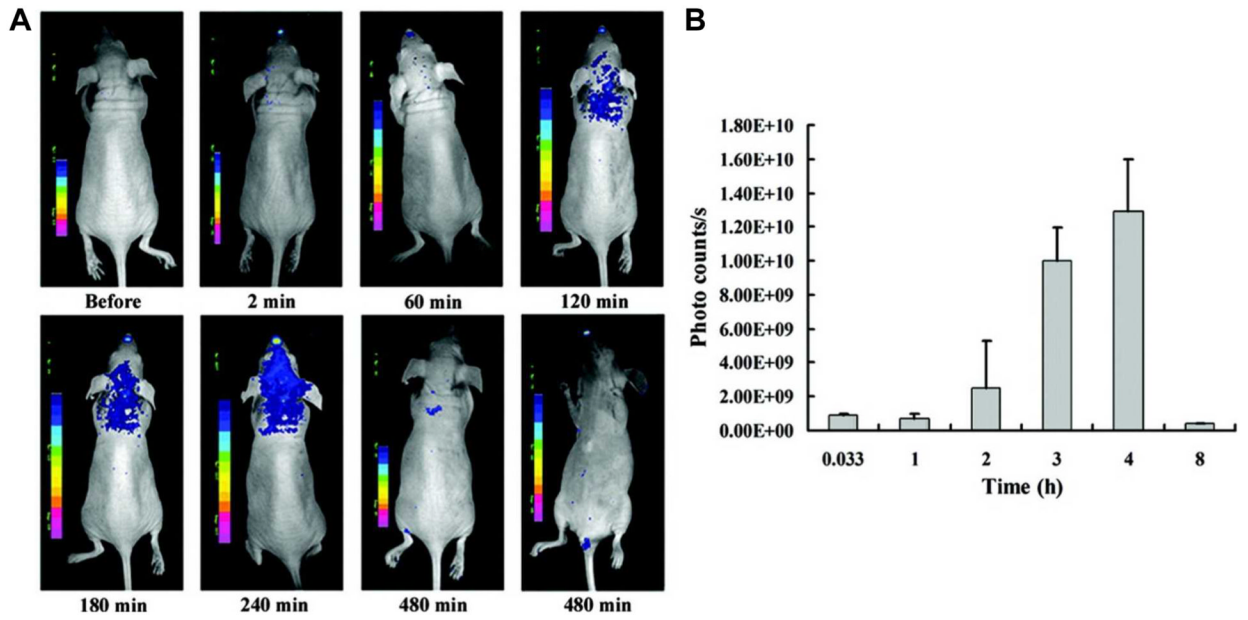


**Fig. (7).**  
**(A)** Distribution and retention of wheat germ agglutinin-conjugated QDs in the brain after intranasal injection into mice. **(B)** Fluorescence signal in the brain peaks at 4 h after injection. Adapted from [157].

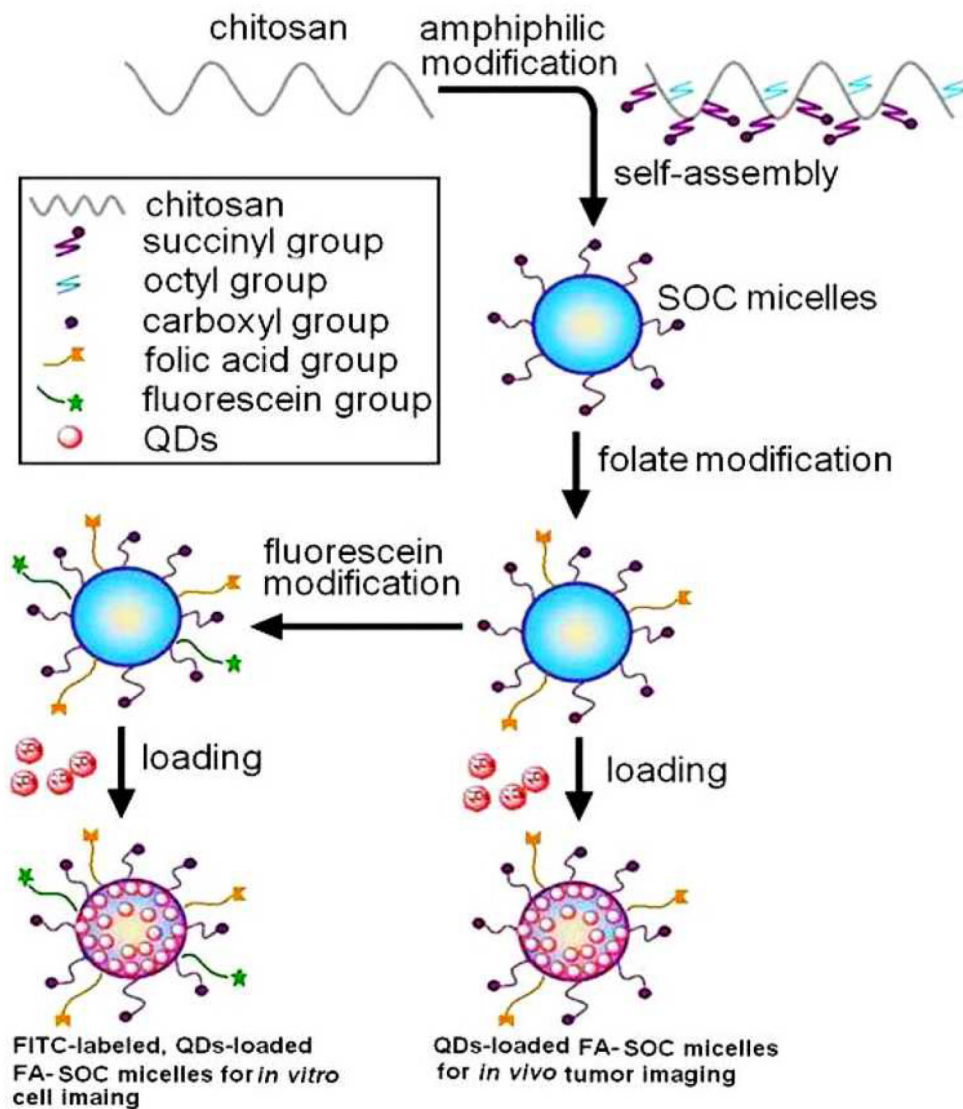


**Fig. (8).** Schematic illustration of the preparation of fluorescently labeled QD-loaded micelles. Adapted from [89].

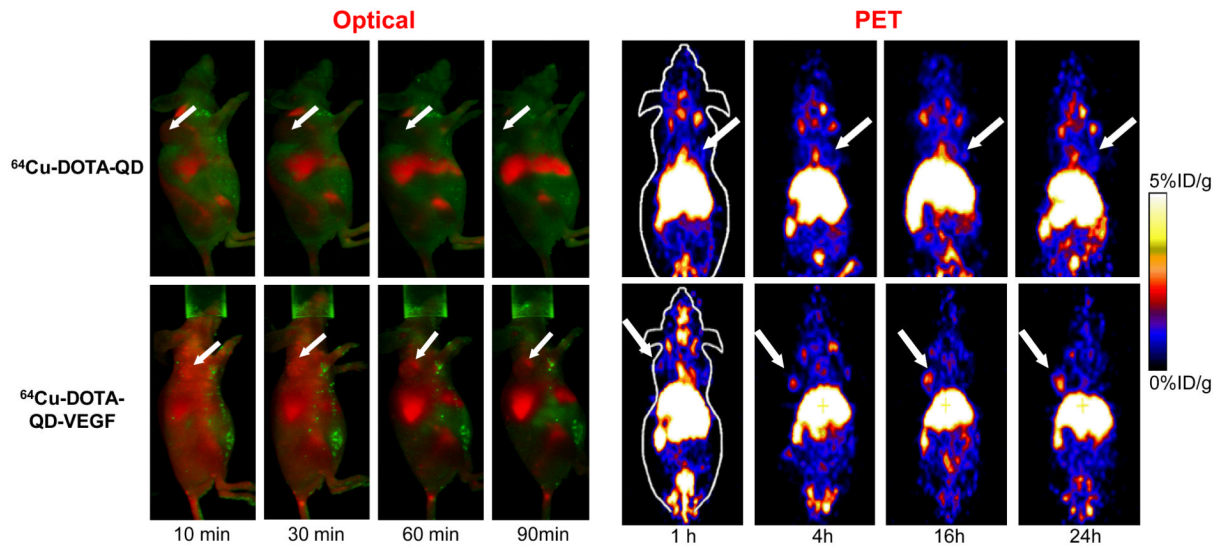


**Fig. (9).** Positron emission tomography (PET) and optical imaging of vascular endothelial growth factor (VEGF) receptor expression in a mouse model using a QD-based dual-modality probe.  $^{64}\text{Cu}$  was used as the radiolabel and VEGF was used as the targeting ligand. Adapted from [184].